DYNAMICS & CONTROL OF UNDERWATER GLIDERS I: STEADY MOTIONS

N. Mahmoudian, J. Geisbert, & C. Woolsey

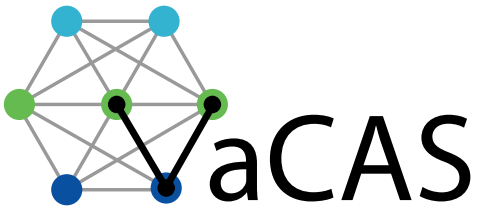

Virginia Center for Autonomous Systems
Virginia Polytechnic Institute & State University
Blacksburg, VA 24060
www.unmanned.vt.edu

June 6, 2009

Technical Report No. VaCAS-2007-01

Summary

This paper describes analysis of steady motions for underwater gliders, a type of highly efficient underwater vehicle which uses gravity for propulsion. Underwater gliders are winged underwater vehicles which locomote by modulating their buoyancy and their attitude. Several such vehicles have been developed and have proven their worth as efficient long-distance, long-duration ocean sampling platforms. To date, the primary emphasis in underwater glider development has been on locomotive efficiency; maneuverability has been a secondary concern. The ultimate aim of our research is to develop optimal motion control strategies which enhance the natural locomotive efficiency of underwater gliders by minimizing the energy expended by the control system. Ambitious applications such as persistent undersea surveillance require not only efficient vehicles, but efficient guidance and control schemes. This technical report aims to develop a better understanding of glider maneuverability, particularly with regard to turning motions. As a preliminary step, we develop an approximate analytical expression for steady turning motion for a realistic glider model. The problem is formulated in terms of regular perturbation theory, with the vehicle turn rate as the perturbation parameter. The resulting solution exhibits a special structure that allows one to apply existing optimal path planning results for planar mobile robots. The ultimate result is a simple, energy-efficient motion control method for underwater gliders.

Contents

List of Figures

List of Tables

1 Nomenclature

$\hat{\cdot}$ = cross product matrix, $\hat{\boldsymbol{a}}\boldsymbol{b} = \boldsymbol{a} \times \boldsymbol{b}$
$\bar{\cdot}$ = nondimensional value
$\mathbf{0}$ = zero vector
$\mathbf{0}$ = zero matrix
$\mathbb{1}$ = identity matrix
$\boldsymbol{b}_i$ = basis vector for body frame, $i \in \{1, 2, 3\}$
$\boldsymbol{C}_{\mathrm{f}}$ = hydrodynamic coupling matrix
$\mathcal{D}$ = drag force
$\boldsymbol{D}_{\omega}$ = angular rate damping matrix
$\boldsymbol{e}_i$ = basis vector for $\mathbb{R}^3$, $i \in \{1, 2, 3\}$
$\boldsymbol{F}_{\mathrm{visc}}$ = viscous force, $[X,\ Y,\ Z]^T$
g = acceleration due to gravity
$\boldsymbol{h}$ = angular momentum about body origin
$\boldsymbol{i}_i$ = basis vector for inertial frame, $i \in \{1, 2, 3\}$
$\boldsymbol{I}_{\mathrm{rb}}$ = rigid body inertia
$\boldsymbol{I}_{\mathrm{f}}$ = added inertia
l = reference length
$\mathcal{L}$ = lift force
m = mass of displaced fluid
m_{rb} = mass of rigid body *less* particle m_{p}
m_{p} = lateral mass particle
m_{v} = total vehicle mass
$\tilde{m}$ = excess mass, $m_{\mathrm{v}} - m$
$\boldsymbol{M}_{\mathrm{f}}$ = added mass matrix
$\boldsymbol{p}$ = translational momentum
P_{dyn} = dynamic pressure, $\frac{1}{2}\rho V^2$
$\boldsymbol{r}_{\mathrm{p}}$ = position of m_{p}
$\boldsymbol{r}_{\mathrm{rb}}$ = body center of mass (less m_{p})
$\boldsymbol{\mathcal{R}}_{\mathrm{IB}}$ = body to inertial rotation
$\boldsymbol{\mathcal{R}}_{\mathrm{BC}}$ = current to body rotation
$\mathcal{S}$ = side force
S = reference area
$\boldsymbol{T}_{\mathrm{visc}}$ = viscous moment, $[L,\ M,\ N]^T$
$\boldsymbol{v}$ = translational velocity, $[u,\ v,\ w]^T$
V = speed, $\|\boldsymbol{v}\|$
$\boldsymbol{X}$ = inertial position, $[x,\ y,\ z]^T$
α = angle of attack, $\arctan(w/u)$
β = sideslip angle, $\arcsin(v/V)$
δr = rudder angle
ϵ = perturbation parameter
ρ = density
$\boldsymbol{\omega}$ = angular velocity, $[p,\ q,\ r]^T$
ω = angular rate, $\|\boldsymbol{\omega}\|$
$\boldsymbol{\Theta}$ = Euler angles, $[\phi,\ \theta,\ \psi]^T$
$\boldsymbol{\zeta}$ = tilt vector, $\boldsymbol{\mathcal{R}}_{\mathrm{IB}}^T \boldsymbol{i}_3$

Subscripts

0 = nominal value
eq = equilibrium value
rb = rigid body
f = fluid
p = lateral mass particle

In addition to the nomenclature described above, we adopt a slightly modified standard notation for the dimensional and non-dimensional hydrodynamic parameters (the "stability derivatives"). These parameters can be separated into inviscid (potential flow) terms and viscous terms. The inviscid hydrodynamic parameters are the components of the generalized added inertia matrix. In notation similar to that defined by SNAME [11][1], the generalized added inertia matrix is

[1] In SNAME notation, roll moment is denoted by K rather than L

$$\left(\begin{array}{c|c} \boldsymbol{M}_{\mathrm{f}} & \boldsymbol{C}_{\mathrm{f}}^{T} \\ \hline \boldsymbol{C}_{\mathrm{f}} & \boldsymbol{I}_{\mathrm{f}} \end{array}\right) = -\left(\begin{array}{ccc:ccc} X_{\dot{u}} & X_{\dot{v}} & X_{\dot{w}} & X_{\dot{p}} & X_{\dot{q}} & X_{\dot{r}} \\ Y_{\dot{u}} & Y_{\dot{v}} & Y_{\dot{w}} & Y_{\dot{p}} & Y_{\dot{q}} & Y_{\dot{r}} \\ Z_{\dot{u}} & Z_{\dot{v}} & Z_{\dot{w}} & Z_{\dot{p}} & Z_{\dot{q}} & Z_{\dot{r}} \\ \hdashline L_{\dot{u}} & L_{\dot{v}} & L_{\dot{w}} & L_{\dot{p}} & L_{\dot{q}} & L_{\dot{r}} \\ M_{\dot{u}} & M_{\dot{v}} & M_{\dot{w}} & M_{\dot{p}} & M_{\dot{q}} & M_{\dot{r}} \\ N_{\dot{u}} & N_{\dot{v}} & N_{\dot{w}} & N_{\dot{p}} & N_{\dot{q}} & N_{\dot{r}} \end{array}\right)$$

The following table provides definitions of nondimensional quantities used to represent viscous effects. These definitions follow standard aircraft convention, with minor exceptions (such as the use of a single characteristic length l).

Dimensional Quantity	Dimensional Divisor	Nondimensional Quantity
X, Y, Z, $\mathcal{D}$, $\mathcal{L}$	$\frac{1}{2}\rho V^2 S$	C_X, C_Y, C_Z, C_D, C_L
L, M, N	$\frac{1}{2}\rho V^2 S l$	C_l, C_m, C_n
u, v, w	V	$\bar{u}$, $\bar{v}$, $\bar{w}$
p, q, r	V/l	$\bar{p}$, $\bar{q}$, $\bar{r}$

As is standard, we assume that vehicle symmetry decouples the longitudinal and lateral-directional hydrodynamic effects. Specifically, we assume that the longitudinal hydrodynamic forces and moments (X, Z, and M) depend only on longitudinal velocities and accelerations (u, w, and q and their derivatives) and that the lateral-directional hydrodynamic forces and moments (Y, L, and N) depend only on lateral-directional velocities and accelerations (v, p, and q and their derivatives). Notation for the nondimensional stability derivatives, which characterize the viscous hydrodynamic effects, is defined below.

	C_X	C_Z	C_D	C_L	C_m
$\bar{u}$	C_{X_u}	C_{Z_u}	C_{D_u}	C_{L_u}	C_{m_u}
α	C_{X_α}	C_{Z_α}	C_{D_α}	C_{L_α}	C_{m_α}
$\bar{q}$	C_{X_q}	C_{Z_q}	C_{D_q}	C_{L_q}	C_{m_q}

	C_Y	C_l	C_n
β	C_{Y_β}	C_{l_β}	C_{n_β}
$\bar{p}$	C_{Y_p}	C_{l_p}	C_{n_p}
$\bar{r}$	C_{Y_r}	C_{l_r}	C_{n_r}

2 Introduction

For decades, marine scientists and engineers have envisioned the use of autonomous underwater vehicles (AUVs) for long-term, large-scale oceanographic monitoring. However, the propulsion systems and power storage limitations of conventional AUVs do not allow for long-term deployments, at least not without a significant investment in undersea infrastructure to enable recharging. Conventional, battery-powered, propeller-driven AUVs can only operate on the order of a few hours before their power is depleted. Buoyancy driven underwater gliders, on the other hand, have proven to be quite effective for long-range, long-term oceanographic sampling. Gliders are highly efficient winged underwater vehicles which locomote by modifying their internal shape. In a typical configuration, a buoyancy bladder modulates the glider's net weight while one or more moving mass actuators modulate its center of mass relative to the center of buoyancy. By appropriately cycling its actuators, the vehicle can propel itself with great efficiency. The exceptional endurance of underwater gliders is due to their reliance on gravity (weight and buoyancy) for propulsion and attitude control.

The first generation of underwater gliders includes *Seaglider* [9], *Spray* [27], and *Slocum* [34]. These "legacy gliders" were designed with similar functional objectives [7, 17] so they are similar in weight, size, and configuration. Although each legacy glider has demonstrated significantly greater endurance than conventional AUVs, it was recognized in [17] that a change in vehicle configuration could further increase glider efficiency. A prototype of the blended wing-body glider proposed in [17] has been developed jointly by the Scripps Institute of Oceanography's Marine Physical Laboratory and the University of Washington's Applied Physics Laboratory. Potential applications of this vehicle, dubbed the *Liberdade/XRay*, include long-term ocean sampling as well as persistent undersea surveillance.

With the primary emphasis on efficiency, glider maneuverability has been a secondary concern. Applications such as undersea surveillance, however, may require more careful consideration of guidance and control requirements. This technical note builds on the preliminary work in [13] and [2] to provide a better understanding of glider maneuverability, particularly with regard to turning motions. Outcomes will include more effective maneuvering behaviors for existing gliders and improved design guidelines for future underwater gliders. As a preliminary step, we develop an approximate analytical expression for steady turning motion for a realistic glider model. Analytical results, approximate or otherwise, are important for motion planning and control and also for vehicle design, as they may provide guidelines for sizing actuators and stabilizers.

The conditions for steady turning flight of an underwater glider differ significantly from those for an aircraft. Deriving a closed-form expression for the steady turn is quite challenging. Instead, we begin by considering wings level equilibrium flight and consider turning motion as a perturbation. Given a desired equilibrium speed and glide path angle, one may determine the center of gravity (CG) location and the net weight (weight minus buoyant force) required. The resulting longitudinal gliding equilibrium is the nominal solution to a regular perturbation problem in which the vehicle turn rate is the perturbation parameter.

The derivation of analytical conditions for steady turning motions requires a vehicle dynamic model. Nonlinear dynamic models presented in [2, 13, 21] provided the basis for investigations of longitudinal gliding flight. Although the emphasis was on wings level flight, turning motions were also discussed in [13] and [2] and examples were shown for the given vehicle models with chosen parameter values. Bhatta [2] also presented the results of a numerical parametric analysis. No

analytical expressions were provided, however, so it is difficult to make general conclusions about the relationship between parameter values and turning motion characteristics. Here, following a more analytical approach as in [14], we study existence and stability of steady turning motions for general parameter values.

Section 3 develops a dynamic model for an underwater glider. Section 4 gives the conditions for wings level gliding flight. These provide the nominal conditions for a regular perturbation analysis in Section 5, by which approximate conditions for steady turning flight are derived. A numerical case study for the *Slocum* glider is presented in Section 6. Section 7 introduces the problem of optimal motion planning for underwater gliders. Here it is recognized that, by exploiting the special structure of the approximate solution given in Section 5, one may apply existing optimal path planning results obtained for planar mobile robots. A brief summary is given in Section 8.

3 Vehicle Dynamic Model

The glider is modelled as a rigid body of mass $m_{\rm v}$. The vehicle displaces a volume of fluid of mass m. Let $\tilde{m} = m_{\rm v} - m$. If $\tilde{m} = 0$, then the vehicle is neutrally buoyant. If $\tilde{m} > 0$, then the vehicle is heavy in water and tends to sink. If $\tilde{m} < 0$, then the vehicle is buoyant in water and tends to rise. For underwater gliders, $\tilde{m}$ is typically controlled by an inflatable bladder, which changes the value of m by changing the displaced volume.

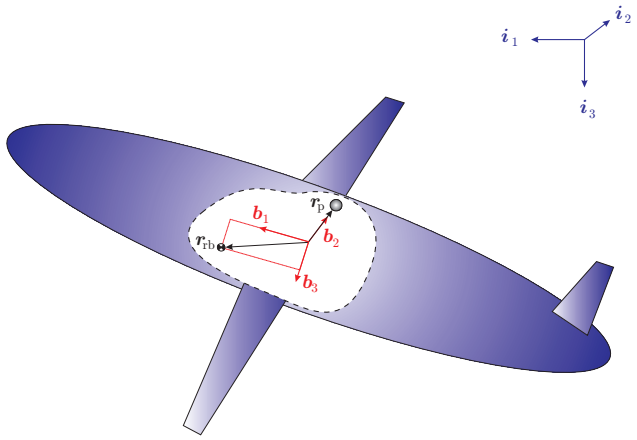

Figure 1: Reference frames.

Referring to Figure 1, the kinematic equations are

$$\dot{\boldsymbol{X}} = \boldsymbol{\mathcal{R}}_{\rm IB}\boldsymbol{v} \tag{1}$$
$$\dot{\boldsymbol{\mathcal{R}}}_{\rm IB} = \boldsymbol{\mathcal{R}}_{\rm IB}\hat{\boldsymbol{\omega}} \tag{2}$$

The rotation matrix $\boldsymbol{\mathcal{R}}_{\rm IB}$ is typically parameterized using the roll angle ϕ, pitch angle θ, and yaw angle ψ:

$$\boldsymbol{\mathcal{R}}_{\rm IB}(\phi,\theta,\psi) = e^{\widehat{\boldsymbol{e}_3}\psi}e^{\widehat{\boldsymbol{e}_2}\theta}e^{\widehat{\boldsymbol{e}_1}\phi} \qquad \text{where} \qquad e^{\boldsymbol{Q}} = \sum_{n=0}^{\infty}\frac{1}{n!}\boldsymbol{Q}^n \quad \text{for} \quad \boldsymbol{Q}\in\mathbb{R}^{n\times n}.$$

Written explicitly,

$$\boldsymbol{\mathcal{R}}_{\mathrm{IB}}(\phi,\theta,\psi) = \begin{pmatrix} \mathrm{c}\theta\mathrm{c}\psi & \mathrm{s}\phi\mathrm{s}\theta\mathrm{c}\psi - \mathrm{c}\phi\mathrm{s}\psi & \mathrm{c}\phi\mathrm{s}\theta\mathrm{c}\psi + \mathrm{s}\phi\mathrm{s}\psi \\ \mathrm{c}\theta\mathrm{s}\psi & \mathrm{c}\phi\mathrm{c}\psi + \mathrm{s}\phi\mathrm{s}\theta\mathrm{s}\psi & -\mathrm{s}\phi\mathrm{c}\psi + \mathrm{c}\phi\mathrm{s}\theta\mathrm{s}\psi \\ -\mathrm{s}\theta & \mathrm{s}\phi\mathrm{c}\theta & \mathrm{c}\phi\mathrm{c}\theta \end{pmatrix}$$

where "s" represents the sine function and "c" represents the cosine function.

In terms of these Euler angles, the kinematic equations (1) and (2) become, respectively,

$$\begin{pmatrix} \dot{x} \\ \dot{y} \\ \dot{z} \end{pmatrix} = \begin{pmatrix} \mathrm{c}\theta\mathrm{c}\psi & \mathrm{s}\phi\mathrm{s}\theta\mathrm{c}\psi - \mathrm{c}\phi\mathrm{s}\psi & \mathrm{c}\phi\mathrm{s}\theta\mathrm{c}\psi + \mathrm{s}\phi\mathrm{s}\psi \\ \mathrm{c}\theta\mathrm{s}\psi & \mathrm{c}\phi\mathrm{c}\psi + \mathrm{s}\phi\mathrm{s}\theta\mathrm{s}\psi & -\mathrm{s}\phi\mathrm{c}\psi + \mathrm{c}\phi\mathrm{s}\theta\mathrm{s}\psi \\ -\mathrm{s}\theta & \mathrm{s}\phi\mathrm{c}\theta & \mathrm{c}\phi\mathrm{c}\theta \end{pmatrix} \begin{pmatrix} u \\ v \\ w \end{pmatrix}$$

$$\begin{pmatrix} \dot{\phi} \\ \dot{\theta} \\ \dot{\psi} \end{pmatrix} = \begin{pmatrix} 1 & \sin\phi\tan\theta & \cos\phi\tan\theta \\ 0 & \cos\phi & -\sin\phi \\ 0 & \sin\phi\sec\theta & \cos\phi\sec\theta \end{pmatrix} \begin{pmatrix} p \\ q \\ r \end{pmatrix}.$$

The angular momentum of the body/fluid system about the body frame origin is denoted by the body vector $\boldsymbol{h}$. The linear momentum of the body/fluid system is denoted by the body vector $\boldsymbol{p}$. The vectors $\boldsymbol{h}$ and $\boldsymbol{p}$ are the conjugate momenta corresponding to $\boldsymbol{\omega}$ and $\boldsymbol{v}$, respectively. To develop expressions for $\boldsymbol{h}$ and $\boldsymbol{p}$ in terms of $\boldsymbol{\omega}$ and $\boldsymbol{v}$ requires a number of definitions.

For simplicity, we assume that $\boldsymbol{r}_{\mathrm{rb}} \cdot \boldsymbol{e}_2 = 0$, so that the vehicle center of mass (less the contribution of m_{p}) is located in the $\boldsymbol{b}_1$-$\boldsymbol{b}_3$ plane. We also assume that $\boldsymbol{r}_{\mathrm{p}} = r_{\mathrm{p}}\boldsymbol{e}_2$, so that that the mass m_{p} is located somewhere along the $\boldsymbol{b}_2$-axis. See Figure 1. Because this technical report only concerns steady motions, we do not consider the internal dynamics of the moving mass actuator; the position of m_{p} is treated as a parameter. See [22] and references cited there for more information on multi-body dynamic models for underwater gliders.

The inertia matrix $\boldsymbol{I}$ is the sum of three components: the *added inertia matrix* $\boldsymbol{I}_{\mathrm{f}}$, the *rigid body inertia matrix* $\boldsymbol{I}_{\mathrm{rb}}$, and a third matrix $-m_{\mathrm{p}}\hat{\boldsymbol{r}}_{\mathrm{p}}\hat{\boldsymbol{r}}_{\mathrm{p}}$. The added inertia accounts for energy necessary to accelerate the fluid as the body rotates. If the underwater glider's external geometry is such that the $\boldsymbol{b}_1$-$\boldsymbol{b}_2$ and $\boldsymbol{b}_1$-$\boldsymbol{b}_3$ planes are planes of symmetry, the added inertia matrix is diagonal:

$$\boldsymbol{I}_{\mathrm{f}} = -\mathrm{diag}\begin{pmatrix} L_{\dot{p}} & M_{\dot{q}} & N_{\dot{r}} \end{pmatrix}.$$

The rigid body inertia represents the distribution of mass m_{rb}; it does not include the contribution of m_{p}, which is accounted for elsewhere. This matrix takes the form

$$\boldsymbol{I}_{\mathrm{rb}} = \begin{pmatrix} I_{xx} & 0 & -I_{xz} \\ 0 & I_{yy} & 0 \\ -I_{xz} & 0 & I_{zz} \end{pmatrix},$$

where the off-diagonal terms in $\boldsymbol{I}$ arise, for example, from an offset center of mass $\boldsymbol{r}_{\mathrm{rb}}$. To summarize,

$$\boldsymbol{I} = \boldsymbol{I}_{\mathrm{f}} + \boldsymbol{I}_{\mathrm{rb}} - m_{\mathrm{p}}\hat{\boldsymbol{r}}_{\mathrm{p}}\hat{\boldsymbol{r}}_{\mathrm{p}}.$$

The mass matrix $\boldsymbol{M}$ is the sum of the *added mass matrix* $\boldsymbol{M}_{\mathrm{f}}$ and $m_{\mathrm{v}}\mathbb{1}$. The added mass matrix accounts for the energy necessary to accelerate the fluid as the body translates. Like the added inertia matrix, the added mass matrix is diagonal for the class of underwater gliders considered here:

$$\boldsymbol{M}_{\mathrm{f}} = -\mathrm{diag}\begin{pmatrix} X_{\dot{u}} & Y_{\dot{v}} & Z_{\dot{w}} \end{pmatrix}.$$

To summarize,

$$\boldsymbol{M} = \boldsymbol{M}_{\mathrm{f}} + m_{\mathrm{v}}\mathbb{1}.$$

In addition to the added inertia and the added mass, there will generally be potential flow and inertial coupling between translational and rotational kinetic energy. The coupling is characterized by the matrix $\boldsymbol{C} = \boldsymbol{C}_{\mathrm{f}} + \boldsymbol{C}_{\mathrm{rb}}$. For the class of underwater gliders considered here,

$$\boldsymbol{C}_{\mathrm{f}} = -\begin{pmatrix} 0 & 0 & 0 \\ 0 & 0 & M_{\dot{w}} \\ 0 & N_{\dot{v}} & 0 \end{pmatrix} = -\begin{pmatrix} 0 & 0 & 0 \\ 0 & 0 & Y_{\dot{r}} \\ 0 & Z_{\dot{q}} & 0 \end{pmatrix}^T$$

and

$$\boldsymbol{C}_{\mathrm{rb}} = m_{\mathrm{rb}}\hat{\boldsymbol{r}}_{\mathrm{rb}} + m_{\mathrm{p}}\hat{\boldsymbol{r}}_{\mathrm{p}} = -\boldsymbol{C}_{\mathrm{rb}}^T.$$

We note that, while the terms appearing in $\boldsymbol{C}_{\mathrm{f}}$ may be significant, they do not appear in previous glider analysis.

The combined rigid body and fluid kinetic energy is therefore

$$\begin{aligned} \mathrm{KE} &= \mathrm{KE}_{\mathrm{f}} + \mathrm{KE}_{\mathrm{rb}} \\ &= \frac{1}{2}\begin{pmatrix} \boldsymbol{v} \\ \boldsymbol{\omega} \end{pmatrix}^T \begin{pmatrix} \boldsymbol{M}_{\mathrm{f}} & \boldsymbol{C}_{\mathrm{f}}^T \\ \boldsymbol{C}_{\mathrm{f}} & \boldsymbol{I}_{\mathrm{f}} \end{pmatrix}\begin{pmatrix} \boldsymbol{v} \\ \boldsymbol{\omega} \end{pmatrix} + \frac{1}{2}\begin{pmatrix} \boldsymbol{v} \\ \boldsymbol{\omega} \end{pmatrix}^T \begin{pmatrix} \boldsymbol{M}_{\mathrm{rb}} & \boldsymbol{C}_{\mathrm{rb}}^T \\ \boldsymbol{C}_{\mathrm{rb}} & \boldsymbol{I}_{\mathrm{rb}} \end{pmatrix}\begin{pmatrix} \boldsymbol{v} \\ \boldsymbol{\omega} \end{pmatrix} \\ &= \frac{1}{2}\begin{pmatrix} \boldsymbol{v} \\ \boldsymbol{\omega} \end{pmatrix}^T \begin{pmatrix} \boldsymbol{M} & \boldsymbol{C}^T \\ \boldsymbol{C} & \boldsymbol{I} \end{pmatrix}\begin{pmatrix} \boldsymbol{v} \\ \boldsymbol{\omega} \end{pmatrix} \end{aligned}$$

The momenta $\boldsymbol{h}$ and $\boldsymbol{p}$ are defined by the kinetic energy metric and the velocities $\boldsymbol{\omega}$ and $\boldsymbol{v}$:

$$\begin{pmatrix} \boldsymbol{p} \\ \boldsymbol{h} \end{pmatrix} = \begin{pmatrix} \boldsymbol{M} & \boldsymbol{C}^T \\ \boldsymbol{C} & \boldsymbol{I} \end{pmatrix}\begin{pmatrix} \boldsymbol{v} \\ \boldsymbol{\omega} \end{pmatrix}. \tag{3}$$

The dynamic equations, which relate external forces and moments to the rate of change of linear and angular momentum, are

$$\dot{\boldsymbol{p}} = \boldsymbol{p}\times\boldsymbol{\omega} + \tilde{m}g\left(\boldsymbol{\mathcal{R}}_{\mathrm{IB}}^T\boldsymbol{i}_3\right) + \boldsymbol{F}_{\mathrm{visc}} \tag{4}$$

$$\dot{\boldsymbol{h}} = \boldsymbol{h}\times\boldsymbol{\omega} + \boldsymbol{p}\times\boldsymbol{v} + (m_{\mathrm{p}}g\boldsymbol{r}_{\mathrm{p}} + m_{\mathrm{rb}}g\boldsymbol{r}_{\mathrm{rb}})\times\left(\boldsymbol{\mathcal{R}}_{\mathrm{IB}}^T\boldsymbol{i}_3\right) + \boldsymbol{T}_{\mathrm{visc}}. \tag{5}$$

The terms $\boldsymbol{T}_{\mathrm{visc}}$ and $\boldsymbol{F}_{\mathrm{visc}}$ represent external moments and forces which do not derive from scalar potential functions. These moments and forces include control moments, such as the yaw moment due to a rudder, and viscous forces, such as lift and drag.

The viscous force and moment are most easily expressed in the "current" reference frame. This frame is related to the body frame through the proper rotation

$$\boldsymbol{\mathcal{R}}_{\mathrm{BC}}(\alpha,\beta) = e^{-\widehat{\boldsymbol{e}_2}\alpha}e^{\widehat{\boldsymbol{e}_3}\beta} = \begin{pmatrix} \cos\alpha\cos\beta & -\cos\alpha\sin\beta & -\sin\alpha \\ \sin\beta & \cos\beta & 0 \\ \sin\alpha\cos\beta & -\sin\alpha\sin\beta & \cos\alpha \end{pmatrix}.$$

For example, one may write

$$\boldsymbol{v} = \boldsymbol{\mathcal{R}}_{\mathrm{BC}}(\alpha,\beta)(V\boldsymbol{e}_1) = \begin{pmatrix} V\cos\alpha\cos\beta \\ V\sin\beta \\ V\sin\alpha\cos\beta \end{pmatrix}.$$

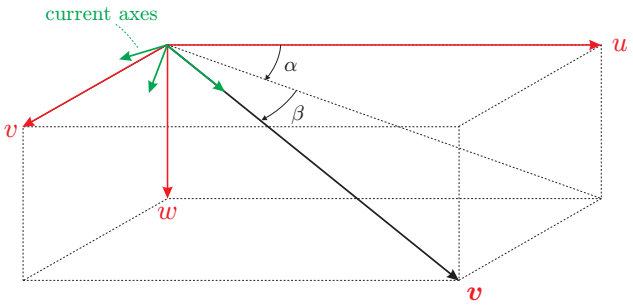

Figure 2: Illustration of the aerodynamic angles.

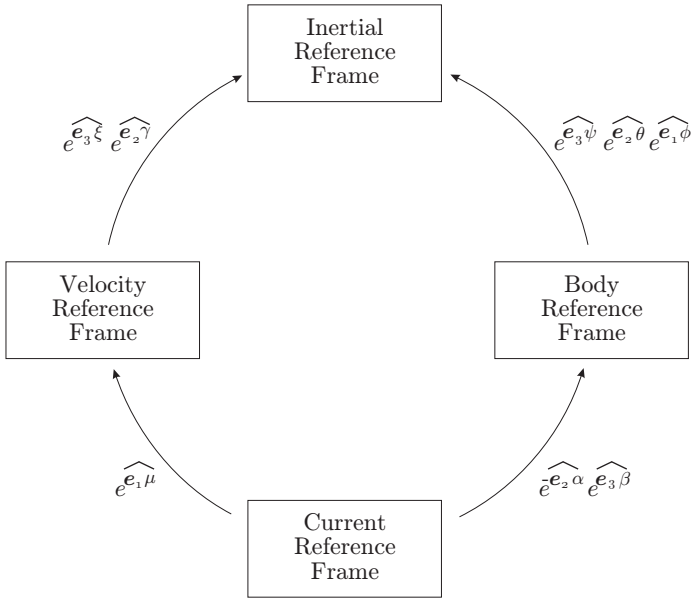

Figure 3: Rotational transformations between various reference frames. (Adapted from [29].)

Transformations between various reference frames of interest in vehicle dynamics are illustrated in Figure 3. The most commonly used reference frames are the inertial, body, and current reference frames, as defined here. Also depicted is the velocity reference frame which is related to the current frame through the bank angle μ and to the inertial frame through the flight path angle γ and the heading angle ζ. (See [29] for details and formal definitions of μ, γ, and ζ.)

The viscous force and moment are assumed to take the following form:

$$\boldsymbol{F}_{\text{visc}} = -\boldsymbol{\mathcal{R}}_{\text{BC}}(\alpha,\beta)\begin{pmatrix} \mathcal{D}(\alpha) \\ \mathcal{S}_\beta \beta + \mathcal{S}_{\delta r}\delta r \\ \mathcal{L}_\alpha \alpha \end{pmatrix} \quad \text{and} \quad \boldsymbol{T}_{\text{visc}} = \boldsymbol{D}_\omega \boldsymbol{\omega} + \begin{pmatrix} L_\beta \beta \\ M_\alpha \alpha \\ N_\beta \beta + N_{\delta r}\delta r \end{pmatrix}.$$

The various coefficients, such as $\mathcal{L}_\alpha$ and N_β, depend on the vehicle's speed, through the dynamic pressure, the geometry, and the Reynolds number. The matrix $\boldsymbol{D}_\omega$ contains terms which characterize viscous angular damping (such as pitch and yaw damping). The expressions above reflect several common assumptions:

- The zero-β side force vanishes (when $\delta r = 0$).

- The zero-α lift force vanishes and the zero-α viscous pitch moment is zero.
- The viscous lift and side forces are linear in α and β, respectively.
- The viscous drag force is quadratic in lift (and therefore in α).

Equations (1), (2), (4), and (5) completely describe the motion of a rigid underwater glider in inertial space. In studying steady motions, we typically neglect the translational kinematics (1). Moreover, the structure of the dynamic equations (4) and (5) is such that we only need to retain a portion of the rotational kinematics (2). Given the tilt vector $\boldsymbol{\zeta} = \boldsymbol{\mathcal{R}}_{\mathrm{IB}}^{T}\boldsymbol{i}_3$, and referring to equation (2), it is easy to see that $\dot{\boldsymbol{\zeta}} = \boldsymbol{\zeta} \times \boldsymbol{\omega}$. We therefore consider the following, reduced set of equations:

$$\dot{\boldsymbol{\zeta}} = \boldsymbol{\zeta} \times \boldsymbol{\omega} \tag{6}$$

$$\dot{\boldsymbol{p}} = \boldsymbol{p} \times \boldsymbol{\omega} + \tilde{m} g \boldsymbol{\zeta} + \boldsymbol{F}_{\mathrm{visc}}. \tag{7}$$

$$\dot{\boldsymbol{h}} = \boldsymbol{h} \times \boldsymbol{\omega} + \boldsymbol{p} \times \boldsymbol{v} + (m_{\mathrm{p}} g \boldsymbol{r}_{\mathrm{p}} + m_{\mathrm{rb}} g \boldsymbol{r}_{\mathrm{rb}}) \times \boldsymbol{\zeta} + \boldsymbol{T}_{\mathrm{visc}} \tag{8}$$

The steady-state flight conditions are determined by solving the nonlinear state equations (6-8) for the state and control vectors that make the state derivatives identically zero. Because of the complexity involved in computing an analytical solution, numerical algorithms for computing "trim conditions" are common [30]. Here we take an analytical approach to find (approximate) solutions for steady-state flight in terms of the model parameters. First, the case of wings-level gliding flight is reviewed. Then, steady turning (helical) flight is analyzed.

4 Wings Level Gliding Flight

The conditions for wings level, gliding flight are that $\boldsymbol{\omega} = \boldsymbol{0}$, $\boldsymbol{v} \cdot \boldsymbol{e}_2 = 0$, and $\boldsymbol{\zeta} \cdot \boldsymbol{e}_2 = 0$. The second condition implies that $v = 0$ and therefore that $\beta = 0$. The third condition implies that $\phi = 0$. Also, we require that $r_{\mathrm{p}} = 0$ and that $\delta r = 0$. Inserting these conditions into equations (7) and (8) and solving for the remaining equilibrium conditions gives:

$$\boldsymbol{0} = \tilde{m} g \boldsymbol{\zeta}_0 + \begin{pmatrix} -\mathcal{D}(\alpha_0)\cos\alpha_0 + \mathcal{L}_\alpha \alpha_0 \sin\alpha_0 \\ 0 \\ -\mathcal{D}(\alpha_0)\sin\alpha_0 - \mathcal{L}_\alpha \alpha_0 \cos\alpha_0 \end{pmatrix} \tag{9}$$

$$\boldsymbol{0} = \boldsymbol{M}\boldsymbol{v}_0 \times \boldsymbol{v}_0 + (m_{\mathrm{rb}} g \boldsymbol{r}_{\mathrm{rb}}) \times \boldsymbol{\zeta}_0 + \begin{pmatrix} 0 \\ M_\alpha \alpha_0 \\ 0 \end{pmatrix}. \tag{10}$$

Following the analysis in [14], one may use equation (10) to show that

$$\boldsymbol{r}_{\mathrm{rb}} = \boldsymbol{r}^{\perp} + \varrho \boldsymbol{\zeta}_0 \tag{11}$$

where

$$\boldsymbol{r}^{\perp} = \frac{1}{m_{\mathrm{rb}} g} \left(\boldsymbol{M}\boldsymbol{v}_0 \times \boldsymbol{v}_0 + \begin{pmatrix} 0 \\ M_\alpha \alpha_0 \\ 0 \end{pmatrix} \right) \times \boldsymbol{\zeta}_0.$$

The free parameter ϱ is a measure of how bottom-heavy the vehicle is in a given, wings level flight condition. This parameter plays an important role in determining longitudinal stability of the gliding equilibrium. Note that $\boldsymbol{r} = \boldsymbol{r}^{\perp}$ is a particular solution to the linear algebraic system

$$\hat{\boldsymbol{\zeta}}_0 \boldsymbol{r} = \frac{1}{m_{\mathrm{rb}} g} \left(\boldsymbol{M} \boldsymbol{v}_0 \times \boldsymbol{v}_0 + \begin{pmatrix} 0 \\ M_\alpha \alpha_0 \\ 0 \end{pmatrix} \right)$$

obtained from (10) for which $\boldsymbol{r}^{\perp} \cdot \boldsymbol{\zeta}_0 = 0$. The null space of $\hat{\boldsymbol{\zeta}}_0$ is described by $\varrho \boldsymbol{\zeta}_0$ where $\varrho \in \mathbb{R}$.

Next, one may solve (9) for $\boldsymbol{\zeta}_0$, $\boldsymbol{v}_0$, and $\tilde{m}_0$ given a desired speed V_0 and a desired *glide path angle* $\gamma_0 = \theta_0 - \alpha_0$. Expressed in the inertial frame, equation (9) gives

$$\begin{pmatrix} 0 \\ 0 \\ \tilde{m} g \end{pmatrix} = \begin{pmatrix} \sin(\gamma_0) \mathcal{L}_\alpha \alpha_0 + \cos(\gamma_0) \mathcal{D}(\alpha_0) \\ 0 \\ \cos(\gamma_0) \mathcal{L}_\alpha \alpha_0 - \sin(\gamma_0) \mathcal{D}(\alpha_0) \end{pmatrix}. \tag{12}$$

Equation (12) states that there is no net hydrodynamic force in the $\boldsymbol{i}_1$-direction and that net weight is balanced by the vertical components of the lift and drag forces.

The components of viscous force, in the current frame, are

$$\mathcal{D}(\alpha) = P_{\mathrm{dyn}} S C_D(\alpha), \qquad \mathcal{S}(\beta) = P_{\mathrm{dyn}} S C_S(\beta), \qquad \text{and} \qquad \mathcal{L}(\alpha) = P_{\mathrm{dyn}} S C_L(\alpha)$$

where, following standard assumptions, the nondimensional coefficients take the form

$$C_D(\alpha) = C_{D_0} + K C_L(\alpha)^2, \qquad C_S(\beta) = C_{S_\beta} \beta, \qquad \text{and} \qquad C_L(\alpha) = C_{L_\alpha} \alpha.$$

The first component of equation (12) may be re-written as

$$\begin{aligned} \tan(\gamma_0) &= -\frac{C_D(\alpha_0)}{C_L(\alpha_0)} \\ &= -\left(\frac{C_{D_0} + K C_L(\alpha_0)^2}{C_L(\alpha_0)} \right) \end{aligned}$$

which implies that

$$K C_L^2 + \tan(\gamma_0) C_L + C_{D_0} = 0. \tag{13}$$

Note that a given glide path angle γ can be obtained, i.e., a real solution C_L to equation (13) exists, if and only if

$$\tan^2(\gamma_0) \geq 4 K C_{D_0}.$$

Thus, for upward glides ($\gamma_0 > 0$), one requires that

$$\gamma_0 \geq \tan^{-1}\left(2\sqrt{K C_{D_0}} \right)$$

while for downward glides, one must choose

$$\gamma_0 \leq -\tan^{-1}\left(2\sqrt{K C_{D_0}} \right).$$

Clearly, the smaller the product $K C_{D_0}$, the larger the range of achievable glide path angles. Given values of K and C_{D_0}, the best possible glide path angle is

$$\gamma_0 = (\pm) \tan^{-1}\left(2\sqrt{K C_{D_0}} \right),$$

This glide path maximizes range (in still water) and corresponds to minimum drag flight:

$$C_L(\alpha_0) = \mp\sqrt{\frac{C_{D_0}}{K}} \qquad \Rightarrow \qquad \alpha_0 = \mp\frac{1}{C_{L_\alpha}}\sqrt{\frac{C_{D_0}}{K}}.$$

These conditions provide an upper bound on achievable performance, but operational considerations may dictate a steeper glide path angle.

Having obtained values for $C_D(\alpha_0)$ and $C_L(\alpha_0)$ (and for α_0 and γ_0, and therefore θ_0), one may solve the third component of equation (12) for the required net weight $\tilde{m}_0 g$ for a given glide speed V_0:

$$\tilde{m}_0 g = \left(\frac{1}{2}\rho V_0^2 S\right)\left(\cos(\gamma_0) C_{L_\alpha}\alpha_0 - \sin(\gamma_0)\left(C_{D_0} + K\left(C_{L_\alpha}\alpha_0\right)^2\right)\right). \tag{14}$$

Thus, one may independently assign the glider's equilibrium attitude, by moving the center of mass according to (11), and its speed, by changing the net weight $\tilde{m}_0 g$ according to (14). For the minimum drag flight condition, for example,

$$\tilde{m}_0 g = \left(\frac{1}{2}\rho V_0^2 S\right)\left(\mp\sqrt{\frac{C_{D_0}}{K}}\cos(\gamma_0) - 2C_{D_0}\sin(\gamma_0)\right).$$

5 Steady Turning Flight

For turning flight, the condition on $\boldsymbol{\omega}$ becomes $\boldsymbol{\omega} \parallel \boldsymbol{\zeta}$. One may therefore write

$$\boldsymbol{\omega} = \omega\boldsymbol{\zeta}$$

where $\omega \in \mathbb{R}$ is the turn rate. A steady turn is an asymmetric flight condition, so we no longer assume that v and ϕ are zero. Moreover, to effect and maintain such an asymmetric flight condition requires that r_p or δr or both be nonzero.

5.1 Turning Flight for Aircraft

Before discussing turning flight for an underwater glider, we first review the conditions for turning flight of aircraft in the notation that we have developed for underwater gliders. Key differences include the hydrodynamic forces (which, for AUVs, include a significant contribution from added mass and inertia) and the force of buoyancy. Since there is no appreciable buoyant force for aircraft, the body frame origin is typically chosen as the center of mass. In this case, the momenta $\boldsymbol{p}$ and $\boldsymbol{h}$ are related to the velocities $\boldsymbol{v}$ and $\boldsymbol{\omega}$ as follows:

$$\begin{pmatrix} \boldsymbol{p} \\ \boldsymbol{h} \end{pmatrix} = \begin{pmatrix} m_\mathrm{rb}\mathbb{1} & \mathbf{0} \\ \mathbf{0} & \boldsymbol{I} \end{pmatrix}\begin{pmatrix} \boldsymbol{v} \\ \omega\boldsymbol{\zeta} \end{pmatrix}. \tag{15}$$

Another important difference between aircraft and underwater gliders is the type of actuation. Aircraft use control surfaces, such as ailerons, a rudder, and an elevator to produce control moments, while underwater gliders use the gravitational moment, which can be adjusted by moving an internal mass.

For an aircraft in a steady turn, equations (6) through (8) simplify to the following:

$$\dot{\boldsymbol{\zeta}} = \mathbf{0} \tag{16}$$

$$\dot{\boldsymbol{p}} = \mathbf{0} = \boldsymbol{p} \times \omega\boldsymbol{\zeta} + m_{\mathrm{rb}} g\boldsymbol{\zeta} + \boldsymbol{F}_{\mathrm{visc}} \tag{17}$$

$$\dot{\boldsymbol{h}} = \mathbf{0} = \boldsymbol{h} \times \omega\boldsymbol{\zeta} + \boldsymbol{T}_{\mathrm{visc}} \tag{18}$$

Note that the first equation implies that $\boldsymbol{\zeta}$ is constant, which means that ϕ and θ are constant. Also note, in the second equation, that the term $\boldsymbol{p} \times \boldsymbol{v}$ has vanished because linear velocity and momentum are parallel for an aircraft.

The viscous forces and moments will be different from those for an underwater glider, of course, and they will include terms due the control surfaces. Thus, terms such as roll moment due to aileron ($L_{\delta a}\delta a$) and coupling between the aileron and rudder ($N_{\delta a}\delta a$ and $L_{\delta r}\delta r$) must be included. Also, angular rate effects on the aerodynamic force and moment are included, with standard assumptions concerning vehicle symmetry.

Let T represent thrust, which is assumed to be aligned with the longitudinal axis. Then

$$\boldsymbol{F}_{\mathrm{visc}} = \begin{pmatrix} X \\ Y \\ Z \end{pmatrix} = -\boldsymbol{\mathcal{R}}_{\mathrm{BC}}(\alpha, \beta) \begin{pmatrix} \mathcal{D}(\alpha, \beta, \delta a, \delta e, \delta r) \\ \mathcal{S}_\beta \beta + \mathcal{S}_{\delta r}\delta r \\ \mathcal{L}_\alpha \alpha + \mathcal{L}_{\delta e}\delta e \end{pmatrix} + \begin{pmatrix} T + X_q q \\ Y_p p + Y_r r \\ Z_q q \end{pmatrix}.$$

For small sideslip angles,

$$Y = Y_\beta \beta + Y_{\delta r}\delta r + Y_p p + Y_r r.$$

The viscous moment takes the form

$$\boldsymbol{T}_{\mathrm{visc}} = \begin{pmatrix} L_\beta \beta + L_{\delta_a}\delta a + L_{\delta_r}\delta r + L_p p + L_r r \\ M_\alpha \alpha + M_{\delta_e}\delta e + M_q q \\ N_\beta \beta + N_{\delta_a}\delta a + N_{\delta_r}\delta r + N_p p + N_r r \end{pmatrix}$$

For steady turning flight, the components of $\boldsymbol{v}$ and $\boldsymbol{\omega}$ are small, with the exception of $u \approx V$. Neglecting products of small terms, one finds that

$$\boldsymbol{p} \times \omega\boldsymbol{\zeta} \approx m_{\mathrm{rb}} V \omega \begin{pmatrix} 0 \\ -\cos\phi\cos\theta \\ \sin\phi\cos\theta \end{pmatrix}_{\mathrm{eq}} \qquad \text{and} \qquad \boldsymbol{h}_{\mathrm{eq}} \times \omega\boldsymbol{\zeta}_{\mathrm{eq}} \approx \mathbf{0}.$$

Substituting into (17) and (18), the conditions for steady turning motion of an aircraft are

$$\mathbf{0} = m_{\mathrm{rb}} V \omega \begin{pmatrix} 0 \\ -\cos\phi\cos\theta_0 \\ \sin\phi\cos\theta_0 \end{pmatrix} + m_{\mathrm{rb}} g \begin{pmatrix} -\sin\theta \\ \sin\phi\cos\theta \\ \cos\phi\cos\theta \end{pmatrix} + \boldsymbol{F}_{\mathrm{visc}} \tag{19}$$

$$\mathbf{0} = \boldsymbol{T}_{\mathrm{visc}} \tag{20}$$

The key condition for steady turning flight is that the lateral aerodynamic force Y be identically zero [10]. From the second component of equation (19), one therefore requires that

$$0 = m_{\mathrm{rb}} V \omega(-\cos\phi\cos\theta) + m_{\mathrm{rb}} g(\sin\phi\cos\theta),$$

from which the roll angle ϕ can be obtained in terms of turn rate ω:

$$\tan\phi = \frac{V}{g}\omega. \tag{21}$$

The pitch angle θ, angle of attack α, and pitch rate q may be determined from the longitudinal components of (19) and (20), as parameterized by the elevator angle δe and thrust T. The remaining conditions for steady turning flight are then obtained from the remaining linear algebraic system:

$$\begin{pmatrix} Y_\beta & Y_{\delta r} & 0 \\ L_\beta & L_{\delta r} & L_{\delta a} \\ N_\beta & N_{\delta r} & N_{\delta a} \end{pmatrix} \begin{pmatrix} \beta \\ \delta r \\ \delta a \end{pmatrix} = \begin{pmatrix} Y_p & Y_r \\ L_p & L_r \\ N_p & N_r \end{pmatrix} \begin{pmatrix} \omega\sin\theta \\ -\omega\cos\theta\cos\phi \end{pmatrix}. \tag{22}$$

These equations give the sideslip angle and aileron and rudder deflections necessary for an aircraft to maintain a banked turn at a given speed V, turn rate ω, and pitch angle θ.

5.2 Turning Flight for Underwater Gliders

The situation for an underwater glider is considerably different. The center of mass is no longer the origin of the body reference frame and angular and linear momentum are coupled through inertial asymmetries. Linear momentum is no longer parallel to linear velocity, because added mass is directional and because of coupling between linear and angular velocity introduced by the offset center of mass. Propulsion is provided not by a thruster but by the net weight of the vehicle (weight minus buoyant force). In fact, the problem of finding analytical steady turning solutions for underwater gliders is quite challenging. We instead formulate the problem as a regular perturbation problem in the turn rate and seek a first order approximate solution. To argue that the higher order solutions are "small corrections" requires some well-founded notion of "small" so we begin by nondimensionalizing the dynamic equations.

We choose the reference parameters

$$\text{length: } l \qquad \text{mass: } m_{\text{rb}} \qquad \text{and} \qquad \text{time: } T = \frac{l}{V_0}$$

where l is a characteristic length scale for the vehicle (such as length overall) and V_0 is the nominal speed. With these definitions, the nondimensional momenta $\bar{\boldsymbol{p}}$ and $\bar{\boldsymbol{h}}$ are related to the nondimensional velocities $\bar{\boldsymbol{v}}$ and $\bar{\boldsymbol{\omega}}$ through the nondimensional generalized inertia matrix as follows:

$$\begin{pmatrix} \bar{\boldsymbol{p}} \\ \bar{\boldsymbol{h}} \end{pmatrix} = \begin{pmatrix} \bar{\boldsymbol{M}} & \bar{\boldsymbol{C}}^T \\ \bar{\boldsymbol{C}} & \bar{\boldsymbol{I}} \end{pmatrix} \begin{pmatrix} \bar{\boldsymbol{v}} \\ \bar{\boldsymbol{\omega}} \end{pmatrix}$$

where

$$\bar{\boldsymbol{v}} = \frac{1}{V_0}\boldsymbol{v} \qquad \text{and} \qquad \bar{\boldsymbol{\omega}} = \boldsymbol{\omega}T$$

and where

$$\bar{\boldsymbol{M}} = \frac{1}{m_{\text{rb}}}\boldsymbol{M}, \qquad \bar{\boldsymbol{I}} = \frac{1}{m_{\text{rb}}l^2}\boldsymbol{I}, \qquad \text{and} \qquad \bar{\boldsymbol{C}} = \frac{1}{m_{\text{rb}}l}\boldsymbol{C}.$$

The nondimensional dynamic equations are

$$\dot{\bar{\boldsymbol{\zeta}}} = \bar{\boldsymbol{\zeta}} \times \bar{\boldsymbol{\omega}} \tag{23}$$

$$\dot{\bar{\boldsymbol{p}}} = \bar{\boldsymbol{p}} \times \bar{\boldsymbol{\omega}} + \bar{\tilde{m}}\bar{\boldsymbol{\zeta}} + \bar{\boldsymbol{F}}_{\text{visc}}. \tag{24}$$

$$\dot{\bar{\boldsymbol{h}}} = \bar{\boldsymbol{h}} \times \bar{\boldsymbol{\omega}} + \bar{\boldsymbol{p}} \times \bar{\boldsymbol{v}} + (\bar{m}_{\text{p}}\bar{\boldsymbol{r}}_{\text{p}} + \bar{\boldsymbol{r}}_{\text{rb}}) \times \bar{\boldsymbol{\zeta}} + \bar{\boldsymbol{T}}_{\text{visc}} \tag{25}$$

where the overdot represents differentiation with respect to nondimensional time T and where

$$\bar{\boldsymbol{\zeta}} = \frac{\boldsymbol{\zeta}}{V_0^2/(gl)}, \quad \bar{\tilde{m}} = \frac{\tilde{m}}{m_{\rm rb}}, \quad \bar{m}_{\rm p} = \frac{m_{\rm p}}{m_{\rm rb}}, \quad \bar{\boldsymbol{r}}_{\rm rb} = \frac{\boldsymbol{r}_{\rm rb}}{l}, \quad \text{and} \quad \bar{\boldsymbol{r}}_{\rm p} = \frac{\bar{\boldsymbol{r}}}{l}$$

and

$$\bar{\boldsymbol{F}}_{\rm visc} = \frac{\boldsymbol{F}_{\rm visc}}{m_{\rm rb}V_0^2/l} \quad \text{and} \quad \bar{\boldsymbol{M}}_{\rm viscous} = \frac{\boldsymbol{T}_{\rm visc}}{m_{\rm rb}V_0^2}.$$

To express the viscous forces and moments explicitly, we also define

$$\bar{V} = \frac{V}{V_0}, \qquad \bar{\rho} = \frac{\rho}{m_{\rm rb}/l^3}, \qquad \text{and} \qquad \bar{S} = \frac{S}{l^2}.$$

To simplify the analysis, we assume that

$$\bar{\boldsymbol{D}}_\omega = \frac{1}{2}\bar{\rho}\bar{V}^2\bar{S}\ \text{diag}\left(C_{l_p},\ C_{m_q},\ C_{n_r}\right)$$

where C_{l_p}, C_{m_q}, and C_{n_r} are nondimensional stability derivatives representing rotational damping. The assumption that roll and yaw damping are decoupled is reasonable for a vehicle with two planes of external geometric symmetry.

Recall that $\bar{\boldsymbol{\omega}} = \bar{\omega}\boldsymbol{\zeta}$ for a steady turn. Define a characteristic frequency $\omega_n = \sqrt{g/l}$ and let $\bar{\omega}_n = \omega_n T$ denote its nondimensional value. Let $\bar{\omega} = \epsilon\bar{\omega}_n$ where ϵ is a small, nondimensional parameter. One may treat the problem of solving for steady turning flight conditions as an algebraic regular perturbation problem in ϵ. When $\epsilon = 0$, the vehicle is in wings-level equilibrium flight. If $\epsilon \neq 0$, then either $r_{\rm p}$ or δr or both must be nonzero. (Recall that $\boldsymbol{r}_{\rm rb}$ remains fixed at its nominal value, which corresponds to the nominal wings-level flight condition when $r_{\rm p}$ and δr are zero.)

Having nondimensionalized the terms appearing in the dynamic equations, we simplify notation by omitting the overbar; in the sequel, all quantities are nondimensional unless otherwise stated. The nondimensional equilibrium equations are

$$\begin{aligned}
\mathbf{0} &= \boldsymbol{p}_{\rm eq} \times \omega\boldsymbol{\zeta}_{\rm eq} + \tilde{m}_{\rm eq}\boldsymbol{\zeta}_{\rm eq} - \left(\frac{1}{2}\rho V_{\rm eq}^2 S\right)\boldsymbol{\mathcal{R}}_{\rm BC}(\alpha_{\rm eq},\beta_{\rm eq})\begin{pmatrix} C_D(\alpha) \\ C_{S_\beta}\beta \\ C_{L_\alpha}\alpha \end{pmatrix}_{\rm eq} \\
\mathbf{0} &= \boldsymbol{h}_{\rm eq} \times \omega\boldsymbol{\zeta}_{\rm eq} + \boldsymbol{p}_{\rm eq} \times \boldsymbol{v}_{\rm eq} + (m_{\rm p}\boldsymbol{r}_{\rm p} + \boldsymbol{r}_{\rm rb}) \times \boldsymbol{\zeta}_{\rm eq} \\
&\qquad + \boldsymbol{D}_\omega\omega\boldsymbol{\zeta}_{\rm eq} + \left(\frac{1}{2}\rho V_{\rm eq}^2 S\right)\begin{pmatrix} C_{l_\beta}\beta \\ C_{m_\alpha}\alpha \\ C_{n_\beta}\beta + C_{n_{\delta r}}\delta r \end{pmatrix}_{\rm eq}
\end{aligned}$$

where C_{l_β}, C_{m_α}, C_{n_β}, and $C_{n_{\delta r}}$ are nondimensional stability derivatives. Note that

$$\begin{pmatrix} \boldsymbol{p}_{\rm eq} \\ \boldsymbol{h}_{\rm eq} \end{pmatrix} = \begin{pmatrix} \boldsymbol{M} & \boldsymbol{C}^T \\ \boldsymbol{C} & \boldsymbol{I} \end{pmatrix}\begin{pmatrix} \boldsymbol{v}_{\rm eq} \\ (\omega\boldsymbol{\zeta}_{\rm eq}) \end{pmatrix}$$

where

$$\boldsymbol{v}_{\rm eq} = \boldsymbol{\mathcal{R}}_{\rm BC}(\alpha_{\rm eq},\beta_{\rm eq})(V_{\rm eq}\boldsymbol{e}_1).$$

As we have stated, $\boldsymbol{\zeta}$ remains constant in turning flight; equivalently, ϕ and θ remain constant. We seek equilibrium solutions for which the perturbed value of $\boldsymbol{\zeta}$ takes the following form:

$$\begin{aligned}\boldsymbol{\zeta}_{\text{eq}} &= e^{-\phi_{\text{eq}}\widehat{\boldsymbol{e}_1}}\boldsymbol{\zeta}_0 \\ &= \begin{pmatrix} 1 & 0 & 0 \\ 0 & \cos\phi_{\text{eq}} & \sin\phi_{\text{eq}} \\ 0 & -\sin\phi_{\text{eq}} & \cos\phi_{\text{eq}} \end{pmatrix} \boldsymbol{\zeta}_0\end{aligned}$$

By construction, the perturbed equilibrium turning motion will have the same pitch angle θ as the corresponding, unperturbed wings level flight condition.

Using the definitions and observations above, the equilibrium equations are

$$\begin{aligned}\mathbf{0} &= \left(\boldsymbol{M}\left(\boldsymbol{\mathcal{R}}_{\text{BC}}(\alpha_{\text{eq}},\beta_{\text{eq}})(V_{\text{eq}}\boldsymbol{e}_1)\right) + \boldsymbol{C}^T\left(\epsilon\omega_n e^{-\phi_{\text{eq}}\widehat{\boldsymbol{e}_1}}\boldsymbol{\zeta}_0\right)\right) \times \left(\epsilon\omega_n e^{-\phi_{\text{eq}}\widehat{\boldsymbol{e}_1}}\boldsymbol{\zeta}_0\right) \\ &\quad + \tilde{m}_{\text{eq}} e^{-\phi_{\text{eq}}\widehat{\boldsymbol{e}_1}}\boldsymbol{\zeta}_0 - \left(\frac{1}{2}\rho V_{\text{eq}}^2 S\right)\boldsymbol{\mathcal{R}}_{\text{BC}}(\alpha_{\text{eq}},\beta_{\text{eq}}) \begin{pmatrix} C_D(\alpha) \\ C_{S_\beta}\beta \\ C_{L_\alpha}\alpha \end{pmatrix}_{\text{eq}} \qquad (26) \\ \mathbf{0} &= \left(\boldsymbol{I}\left(\epsilon\omega_n e^{-\phi_{\text{eq}}\widehat{\boldsymbol{e}_1}}\boldsymbol{\zeta}_0\right) + \boldsymbol{C}\left(\boldsymbol{\mathcal{R}}_{\text{BC}}(\alpha_{\text{eq}},\beta_{\text{eq}})(V_{\text{eq}}\boldsymbol{e}_1)\right)\right) \times \left(\epsilon\omega_n e^{-\phi_{\text{eq}}\widehat{\boldsymbol{e}_1}}\boldsymbol{\zeta}_0\right) \\ &\quad + \left(\boldsymbol{M}\left(\boldsymbol{\mathcal{R}}_{\text{BC}}(\alpha_{\text{eq}},\beta_{\text{eq}})(V_{\text{eq}}\boldsymbol{e}_1)\right) + \boldsymbol{C}^T\left(\epsilon\omega_n e^{-\phi_{\text{eq}}\widehat{\boldsymbol{e}_1}}\boldsymbol{\zeta}_0\right)\right) \times \left(\boldsymbol{\mathcal{R}}_{\text{BC}}(\alpha_{\text{eq}},\beta_{\text{eq}})(V_{\text{eq}}\boldsymbol{e}_1)\right) \\ &\quad + (m_{\text{p}}\boldsymbol{r}_{\text{p}} + \boldsymbol{r}_{\text{rb}}) \times \left(e^{-\phi_{\text{eq}}\widehat{\boldsymbol{e}_1}}\boldsymbol{\zeta}_0\right) + \boldsymbol{D}_\omega\left(\epsilon\omega_n e^{-\phi_{\text{eq}}\widehat{\boldsymbol{e}_1}}\boldsymbol{\zeta}_0\right) \\ &\quad + \left(\frac{1}{2}\rho V_{\text{eq}}^2 S\right)\begin{pmatrix} C_{l_\beta}\beta \\ C_{m_\alpha}\alpha \\ C_{n_\beta}\beta + C_{n_{\delta r}}\delta r \end{pmatrix}_{\text{eq}} \qquad (27)\end{aligned}$$

To obtain the regular perturbation solution in ϵ, first substitute the following polynomial expansions for r_{p}, $\tilde{m}$, ϕ, V, α, and β.

$$\begin{aligned} V &= \sum_n V_n\epsilon^n = V_0 + \epsilon V_1 + \epsilon^2 V_2 + \cdots & \tilde{m} &= \sum_n \tilde{m}_n\epsilon^n = \tilde{m}_0 + \epsilon\tilde{m}_1 + \epsilon^2\tilde{m}_2 + \cdots \\ \alpha &= \sum_n \alpha_n\epsilon^n = \alpha_0 + \epsilon\alpha_1 + \epsilon^2\alpha_2 + \cdots & \phi &= \sum_n \phi_n\epsilon^n = \epsilon\phi_1 + \epsilon^2\phi_2 + \cdots \\ \beta &= \sum_n \beta_n\epsilon^n = \epsilon\beta_1 + \epsilon^2\beta_2 + \cdots & r_{\text{p}} &= \sum_n r_{\text{p}_n}\epsilon^n = \epsilon r_{\text{p}_1} + \epsilon^2 r_{\text{p}_2} + \cdots \end{aligned}$$

(We have suppressed the subscript "eq" for convenience.) Also, let $\delta r = 0 + \epsilon\delta r_1$. (The rudder deflection δr_1 will appear as a free parameter in the solution to the regular perturbation problem.) Substituting these polynomial expansions into equations (26) and (27) and collecting powers of ϵ gives a regular perturbation series in ϵ. Solving the coefficient equation for ϵ^0 gives the nominal, wings level flight conditions. Solving the coefficient equation for ϵ^1 gives approximate values for r_{p}, $\tilde{m}$, ϕ, V, α, and β to first order in ϵ. Let

$$\begin{aligned}\Delta &= (\rho S)^2\left(r_{b_x}\text{c}\theta_0 + r_{b_z}\text{s}\theta_0\right)\left(C_D(\alpha_0) + C_{S_\beta}\right) + \tilde{m}_0(\rho S)\left(C_{n_\beta}\text{c}\theta_0 - C_{l_\beta}\text{s}\theta_0\right) \\ &\quad + 2\tilde{m}_0\left[\left(-X_{\dot{u}} + Y_{\dot{v}}\right)\text{c}\alpha_0\text{c}\theta_0 + \left(-Z_{\dot{w}} + Y_{\dot{v}}\right)\text{s}\alpha_0\text{s}\theta_0\right] \qquad (28)\end{aligned}$$

where "s" represents the sine function and "c" represents cosine. The first order solution to the

regular perturbation problem defined by equations (26) and (27) is:

$$V_1 = 0 \tag{29}$$

$$\alpha_1 = 0 \tag{30}$$

$$\tilde{m}_1 = 0 \tag{31}$$

$$\begin{aligned}\beta_1 = &-\frac{\omega_n}{\Delta}\left\{2\left(r_{b_x}\mathrm{c}\theta_0 + r_{b_z}\mathrm{s}\theta_0\right)\left[\left(m - X_{\dot{u}}\right)\mathrm{c}\alpha_0\mathrm{c}\theta_0 + \left(m - Z_{\dot{w}}\right)\mathrm{s}\alpha_0\mathrm{s}\theta_0\right]\right.\\ &+2\tilde{m}_0\mathrm{c}\theta_0\mathrm{c}(\theta_0 - \alpha_0)N_{\dot{v}} + \tilde{m}_0\left(\rho S\right)\left(C_{l_p}\mathrm{s}^2\theta_0 + C_{n_r}\mathrm{c}^2\theta_0\right)\Big\}\\ &-\frac{\rho S}{\Delta}\left[\tilde{m}_0\mathrm{c}\theta_0 C_{n_{\delta r}}\delta r_1 + \left(r_{b_x}\mathrm{c}\theta_0 + r_{b_z}\mathrm{s}\theta_0\right)C_{S_{\delta r}}\delta r_1\right]\end{aligned} \tag{32}$$

$$\begin{aligned}\phi_1 = &\frac{\omega_n}{4\tilde{m}_0\mathrm{c}\theta_0\Delta}\left[\left(m + \tilde{m}_0 - X_{\dot{u}}\right)\mathrm{c}\alpha_0\mathrm{c}\theta_0 + \left(m + \tilde{m}_0 - Z_{\dot{w}}\right)\mathrm{s}\alpha_0\mathrm{s}\theta_0\right]\\ &+\frac{\rho S}{8\tilde{m}_0\mathrm{c}\theta_0}\left[\left(C_D(\alpha_0) + C_{S_\beta}\right)\beta_1 + \frac{1}{\Delta}C_{S_{\delta r}}\delta r_1\right]\end{aligned} \tag{33}$$

$$\begin{aligned}r_{\mathrm{p}_1} = &\frac{1}{2m_{\mathrm{p}}\Delta}\left\{2\omega_n\left(\rho S\right)\left(r_{b_x}C_{l_\beta} + r_{b_z}C_{n_\beta}\right)\left[\left(m - X_{\dot{u}}\right)\mathrm{c}\alpha_0\mathrm{c}\theta_0 + \left(m - Z_{\dot{w}}\right)\mathrm{s}\alpha_0\mathrm{s}\theta_0\right]\right.\\ &+2\tilde{m}_0\omega_n\left(\rho S\right)\left[C_{l_p}\left(-X_{\dot{u}} + Y_{\dot{v}}\right)\mathrm{c}\alpha_0\mathrm{s}\theta_0 - C_{n_r}\left(-Z_{\dot{w}} + Y_{\dot{v}}\right)\mathrm{s}\alpha_0\mathrm{c}\theta_0\right]\\ &+2\omega_n\mathrm{s}2\alpha_0\left(-Z_{\dot{w}} + Y_{\dot{v}}\right)\left[r_{b_x}\left(m - X_{\dot{u}}\right)\mathrm{c}\theta_0 + r_{b_z}\left(m - Z_{\dot{w}}\right)\mathrm{s}\theta_0\right]\\ &-2\omega_n\left(1 - \mathrm{c}2\alpha_0\right)\left[r_{b_x}\left(m - Z_{\dot{w}}\right)\left(-Z_{\dot{w}} + Y_{\dot{v}}\right)\mathrm{s}\theta_0\right.\\ &\qquad\left.-r_{b_z}\left(m - X_{\dot{u}}\right)\left(-X_{\dot{u}} + Y_{\dot{v}}\right)\mathrm{c}\theta_0\right]\\ &-4\tilde{m}_0\omega_n\mathrm{s}\alpha_0\left\{\left[M_{\dot{w}}\left(-X_{\dot{u}} + Y_{\dot{v}}\right) + N_{\dot{v}}\left(-X_{\dot{u}} + Z_{\dot{w}}\right)\right]\mathrm{c}\alpha_0\mathrm{s}\theta_0\right.\\ &\qquad\left.-M_{\dot{w}}\left(-Z_{\dot{w}} + Y_{\dot{v}}\right)\mathrm{s}\alpha_0\mathrm{s}\theta_0\right\}\\ &+\omega_n\left(\rho S\right)\left\{\left[\tilde{m}_0C_{l_\beta} - r_{b_z}\left(C_D(\alpha_0) + C_{S_\beta}\right)\right]\right.\\ &\qquad\left.\cdot\left[\left(\rho S\right)C_{n_r}\mathrm{c}\theta_0 + 2\left(N_{\dot{v}}\mathrm{c}\alpha_0\mathrm{c}\theta_0 - M_{\dot{w}}\mathrm{s}\alpha_0\mathrm{s}\theta_0\right)\right]\right.\\ &\left.+\left[\tilde{m}_0C_{n_\beta} + r_{b_x}\left(C_D(\alpha_0) + C_{S_\beta}\right)\right]\left[\left(\rho S\right)C_{l_p}\mathrm{s}\theta_0 + 2\left(M_{\dot{w}} + N_{\dot{v}}\right)\mathrm{s}\alpha_0\mathrm{c}\theta_0\right]\right\}\\ &+\left(\rho S\right)C_{n_{\delta r}}\delta r_1\left\{\left(\rho S\right)\left[\tilde{m}_0C_{l_\beta} - r_{b_z}\left(C_D(\alpha_0) + C_{S_\beta}\right)\right]\right.\\ &\qquad\left.-2\tilde{m}_0\left(-Z_{\dot{w}} + Y_{\dot{v}}\right)\mathrm{s}\alpha_0\right\}\\ &+\left(\rho S\right)C_{S_{\delta r}}\delta r_1\left\{\left(\rho S\right)\left(r_{b_x}C_{l_\beta} + r_{b_z}C_{n_\beta}\right)\right.\\ &\qquad\left.\left.+2\left[r_{b_x}\left(-Z_{\dot{w}} + Y_{\dot{v}}\right)\mathrm{s}\alpha_0 + r_{b_z}\left(-X_{\dot{u}} + Y_{\dot{v}}\right)\mathrm{c}\alpha_0\right]\right\}\right\}\end{aligned} \tag{34}$$

The explicit analytical expressions given above, particularly in equations (32-34), provide insight concerning the role of design parameters such as wing sweep angle, vertical stabilizer size, moving mass actuator size, and rudder size in determining a vehicle's turning capability. They also exhibit an interesting structure, which is discussed in Remark 5.1 below.

Remark 5.1 *That V, α, and $\tilde{m}$ remain constant to first order in ϵ suggests that the primary contributors to steady turning motion are lateral mass deflections (r_{p}) and rudder deflections (δr_1) and that these deflections have no first order effect on speed or angle of attack. In practice, it is considerably more costly to change the vehicle's net mass $\tilde{m}$ than to shift its center of gravity. As shown in equation (14), $\tilde{m}$ directly controls speed. So, for example, to maximize glider speed in descent (ascent), one must drive $\tilde{m}$ to its maximum (minimum) value. Fortunately, the problem of controlling directional motion (turn rate) decouples from the problem of controlling longitudinal motion, to first order in ϵ. Thus, one may choose a desired glide path angle and speed, corresponding to some desired rate of progress, and then leave these actuators fixed while controlling directional*

motion separately with the lateral moving mass actuator. As discussed in Section 7, this observation suggests a natural approach to motion control and path planning for underwater gliders.

Remark 5.2 *Note that the rudder deflection δr_1 appears as a free parameter in expressions (29-34). For a rudderless vehicle, one simply sets $\delta r_1 = 0$. Including a rudder, however, provides additional freedom to control the lateral-directional dynamics. For example, using (32), one could adjust the rudder angle so as to zero the sideslip angle, to first order in ϵ, thereby reducing the total drag. (Equation (32) gives guidance for sizing a rudder for this purpose.) Drag reduction is especially critical for underwater gliders, whose primary operational advantage is efficiency. On the other hand, as an external actuator, a rudder is subject to damage or fouling and introduces an additional failure mode into the system.*

Equations (29-34) provide a first order approximation for steady turning motions. To assess stability of the true, neighboring turning motion, one may linearize about the *approximate* equilibrium condition and compute the eigenvalues. Recognizing that the eigenvalues of the resulting time-invariant state matrix depend continuously on its parameters, stability properties of the true equilibrium may be inferred from stability properties of the approximate equilibrium provided that (i) the equilibrium is hyperbolic and (ii) ϵ is small relative to the real part of every eigenvalue. See Section 1.7 of [15] for a brief discussion or Chapter 9 of [16] for more details.

6 Numerical Case Study: *Slocum*

To verify our steady turn predictions for a realistic vehicle model, we have applied the results to a model for *Slocum*, shown in Figure 4, for which hydrodynamic model parameters are given in [2]. We consider perturbations from a wings-level equilibrium flight condition at speed $V_0 = 1.5$ knots and angle of attack $\alpha_0 = 4.3°$, the angle which corresponds to the maximum lift to drag ratio. We assume that $\delta r_1 = 0$, noting that neither *Liberdade/XRay* nor the deep-water ("thermal") version of *Slocum* uses a rudder.

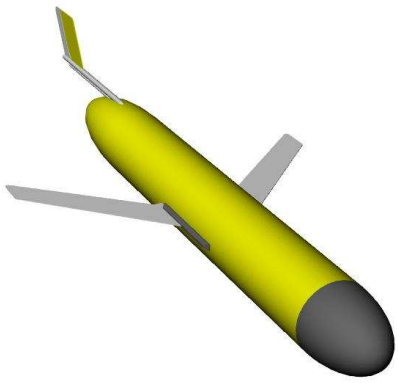

Figure 4: The underwater glider *Slocum*. (Solid model in Rhinoceros 3.0)

Figure 5 shows the wings-level equilibrium glide characteristics for the *Slocum* glider. The lift, sideforce and drag parameters are:

$$C_{L_\alpha} = 2.04 \text{ rad}^{-1}, \qquad C_{S_\beta} = 0.30 \text{ rad}^{-1}, \qquad C_{D_0} = 0.03, \qquad \text{and} \qquad K = 0.16$$

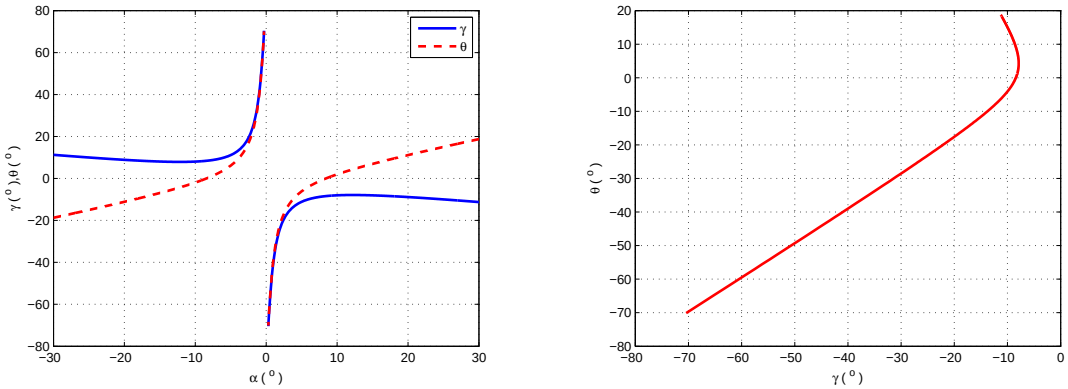

Figure 5: Wings level equilibrium glide characteristics for *Slocum* model.

Other important parameters include $l = 1.5$ m and $m_{\rm rb} = 40$ kg. The values of the nonzero terms in the generalized added mass matrix are given below.

$$-X_{\dot{u}} = 5 \text{ kg} \qquad -L_{\dot{p}} = 3.75 \text{ kg-m}^2$$
$$-Y_{\dot{v}} = 60 \text{ kg} \qquad -M_{\dot{q}} = 2.28 \text{ kg-m}^2$$
$$-Z_{\dot{w}} = 70 \text{ kg} \qquad -N_{\dot{r}} = 1.28 \text{ kg-m}^2$$

The values of the viscous stability derivatives are given below, in the notation defined in the nomenclature section.

	C_m
α	-0.75
$\bar{q}$	-0.90

	C_l
β	-0.90
$\bar{p}$	-0.30

	C_n
β	1.51
$\bar{r}$	-0.30

Once one has computed the conditions for equilibrium flight, one may examine stability. The simplest approach is spectral analysis. Using the *Slocum* model described in [2], we linearize about the wings-level, equilibrium flight condition corresponding to the following parameter values:

$$V_0 = 0.758 \text{ m/s}, \qquad \alpha_0 = 4.3^\circ, \qquad \theta_0 = -8.2^\circ, \qquad \gamma_0 = -12.5^\circ \qquad \text{and} \qquad \tilde{m}_0 = 0.61 \text{ kg}.$$

As mentioned in Section 4, the free parameter ϱ provides a measure of how bottom-heavy the vehicle is, in a given flight condition. This parameter plays an important role in determining longitudinal stability of wings-level gliding equilibria. The effect of varying ϱ on the stability of wings-level and turning equilibria has been investigated numerically. The results show that the equilibrium condition mentioned above is stable provided $\varrho > 0.05$, which agrees with the analysis in Section 8.3 of Bhatta's dissertation [2]. Here, the value of ϱ is fixed at 0.117, as in [2].

The eigenvalues of the state matrix corresponding to the given equilibrium condition are

$$\lambda \in \{-4.46, -2.67 \pm 1.64i, -1.26, -1.03, -0.75 \pm 0.25i, -0.07\}$$

All eight eigenvalues of the linearized system have negative real part, so the flight condition is stable.

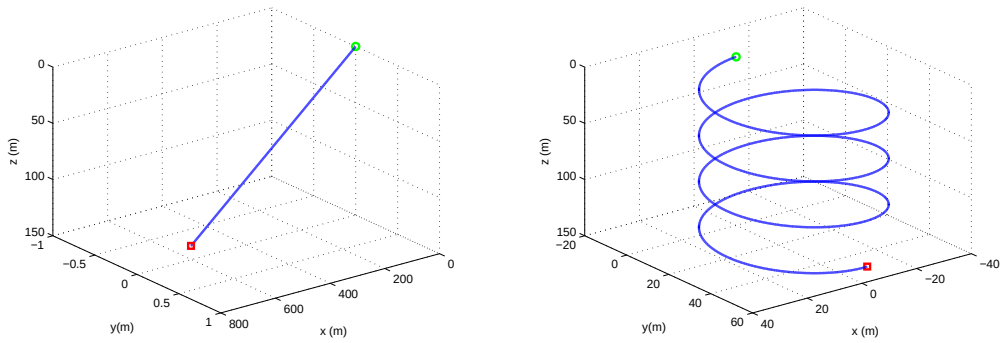

Figure 6: Wings level ($\epsilon = 0$) and turning ($\epsilon = 0.01$) flight paths for the *Slocum* model.

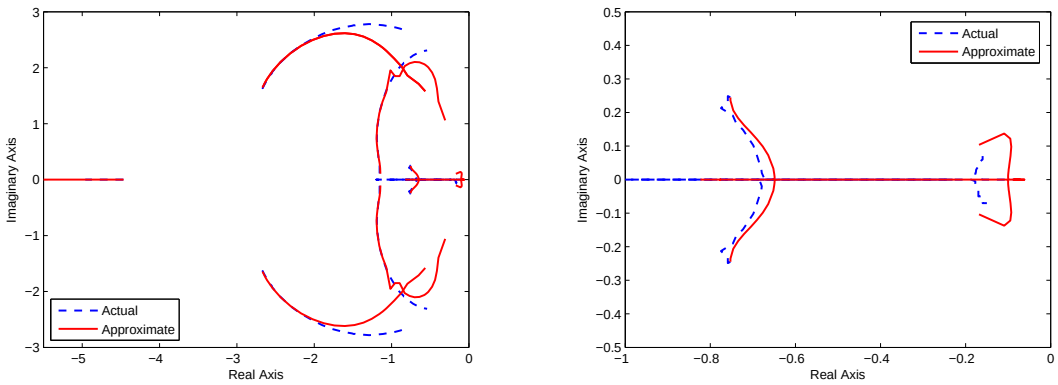

Figure 7: Eigenvalue plots for actual and approximate equilibria for $0 < \epsilon < 0.1$. (A closer view of the dominant eigenvalues is shown at the right.)

With stability of wings-level equilibrium flight confirmed, one may next compute the first order solution for r_{p}, ϕ, and β, as described in Section 5:

$$r_{\mathrm{p}} = (4.63\omega_n\epsilon) \text{ m}, \qquad \phi = (10.06\,\omega_n\epsilon)\left(\frac{180}{\pi}\right) \text{ deg}, \qquad \text{and} \qquad \beta = (0.33\,\omega_n\epsilon)\left(\frac{180}{\pi}\right) \text{ deg}.$$

With these approximate values for lateral mass location, roll angle, and sideslip angle, the approximate equilibrium velocity and angular velocity are

$$\boldsymbol{v} = V_0 \begin{pmatrix} \cos\alpha_0 \cos(\epsilon\beta_1) \\ \sin(\epsilon\beta_1) \\ \cos\alpha_0 \sin(\epsilon\beta_1) \end{pmatrix} \qquad \text{and} \qquad \boldsymbol{\omega} = \omega_n\epsilon \begin{pmatrix} \sin\theta_0 \\ \cos\theta_0 \sin(\epsilon\phi_1) \\ \cos\theta_0 \cos(\epsilon\phi_1) \end{pmatrix}.$$

When $\epsilon = 0$, the values above correspond to the given steady, wings-level flight condition. For small, nonzero values of ϵ, the values correspond (approximately) to a steady turning motion; see Figure 6. To determine the range of stable turning motions that can be obtained using this approximation, the equations of motion are linearized about the approximate turning motion, parameterized by ϵ. When $\epsilon = 0$, all eight eigenvalues of the linearization have negative real part, with $\lambda_8 = -0.07$ being closest to the imaginary axis. As ϵ increases, this eigenvalue moves to the left along the real axis. Two other critical eigenvalues begin as a complex conjugate pair near

the real axis: $\lambda_{6,7} = -0.75 \pm 0.25i$. As ϵ increases from zero, these eigenvalues coalesce at about $-0.6489 \approx -0.65$ and break apart along the real axis. The eigenvalue which becomes less negative eventually coalesces with λ_8 and breaks away into a complex conjugate pair at about -0.1. One may infer that the system has a locally unique, stable fixed point provided ϵ remains smaller in other of magnitudes than magnitude of the real part of the critical eigenvalue(s) [16]. Figure 7 shows the movement of eigenvalues for the approximate equilibrium as well as those for the true equilibrium (computed numerically) as ϵ increases from zero. The true and approximate root loci agree closely for $\epsilon < 0.03$. The true system exhibits a stable turning motion for $0 < \epsilon < 0.1$.

Table 1: Approximate and actual steady motion parameters ($V_0 = 1.5$ kts & α= 4.3°).

ϵ	ϕ (°)		β (°)		θ (°)	V (m/s)	ω (rad/s)		R (m)	
	app.	actual	app.	actual	actual†	actual†	app.	actual	app.	actual
0.001	1.5	1.4	0.1	0.1	-8.7	0.77	0.003	0.003	253.3	256.7
0.005	7.4	7.1	0.2	0.6	-8.8	0.78	0.013	0.014	58.5	55.7
0.01	14.7	13.9	0.5	1.3	-9.0	0.79	0.026	0.027	29.2	29.3
0.03	44.2	35.0	1.5	4.4	-9.8	0.87	0.077	0.057	9.9	15.3
0.05	73.7	47.8	2.4	7.0	-9.7	0.93	0.128	0.063	5.9	14.8
0.07	103.2	56.0	3.4	8.9	-9.0	0.97	0.179	0.060	4.3	16.2

†The approximate value of θ is $\theta_0 = -8.24°$. The approximate value of V is $V_0 = 1.011$ m/s.

Table 1 gives approximate and actual values (obtained from numerical simulations) for key variables for various values of ϵ. Note that, as ϵ increases in value, so does the error between the approximate and true equilibrium values. Regardless, the system does converge to a steady turning motion for all values $\epsilon \leq 0.1$.

Remark 6.1 *Note in Table 1 that the actual turn radius R is minimum around $\epsilon = 0.05$. Since further increases in r_p (or equivalently in ϵ) fail to lower the turn radius, there is no point in moving the particle m_p beyond this critical location. Such an observation may provide guidelines for actuator sizing in future glider designs. There is no reason, for example, to provide moving mass control authority which does not yield greater turning ability.*

Table 2: Approximate and actual steady motion parameters ($V_0 = 2.0$ kts & α= 4.3°).

ϵ	ϕ (°)		β (°)		θ (°)	V (m/s)	ω (rad/s)		R (m)	
	app.	actual	app.	actual	actual†	actual†	app.	actual	app.	actual
0.001	0.9	0.9	0.1	0.1	-8.0	1.00	0.003	0.003	337.0	334.0
0.005	4.3	4.4	0.3	0.3	-8.1	1.00	0.013	0.013	77.8	77.2
0.01	8.7	8.7	0.6	0.6	-8.2	1.01	0.026	0.026	39.6	39.3
0.03	26.1	23.9	2.3	2.3	-9.4	1.07	0.077	0.065	13.2	16.5
0.05	43.4	34.9	3.4	3.6	-10.4	1.14	0.128	0.085	7.9	13.5
0.07	60.8	42.8	4.7	4.9	-10.9	1.21	0.179	0.093	5.7	12.9

†The approximate value of θ is $\theta_0 = -8.24°$. The approximate value of V is $V_0 = 1.011$ m/s.

Comparing the results for speeds of 1.0, 1.5, and 2.0 knots (illustrated in Tables 3, 1, and 2, respectively), one may observe several trends. For example, in every case, actual speed increases with increasing turn rate. (Recall that the approximation suggests that speed remains relatively

Table 3: Approximate and actual steady motion parameters ($V_0 = 1.0$ kt & $\alpha = 4.3°$).

ϵ	ϕ (°)		β (°)		θ (°)	V (m/s)	ω (rad/s)		R (m)	
	app.	actual	app.	actual	actual†	actual†	app.	actual	app.	actual
0.001	2.9	2.8	0.0	0.3	-9.3	0.52	0.003	0.003	170.0	173.3
0.005	14.6	13.5	0.0	1.7	-9.3	0.53	0.013	0.015	39.2	35.3
0.01	29.3	25.4	0.0	3.4	-9.3	0.55	0.026	0.027	19.8	20.9
0.02	58.6	42.7	0.1	9.7	-8.7	0.60	0.051	0.034	9.9	18.0
0.03	87.8	53.5	0.2	12.6	-7.7	0.63	0.077	0.033	6.6	19.5
0.04	117.1	60.7	0.2	13.8	-6.8	0.65	0.102	0.029	5.0	22.0

†The approximate value of θ is $\theta_0 = -8.24°$. The approximate value of V is $V_0 = 0.5056$ m/s.

constant, for small ϵ.) Roll angle and sideslip angle (approximate and actual) increase more rapidly with turn rate at lower nominal speeds than at higher nominal speeds. Moreover, the discrepancy between the approximate and actual values is greatest (for given ϵ) at the lowest speed. Because the relative stability of the nominal flight condition decreases with decreasing speed (i.e., the critical eigenvalues move closer to the imaginary axis), one should expect poorer agreement between the approximation and reality at these lower speeds.

7 Path Planning

A logical next step is to develop a procedure for optimal path planning which makes use of the preceding approximate results for equilibrium turning flight. A reasonable objective would be to concatenate these approximate equilibrium motions in order to minimize the time of transit from a given initial point to a given final point with a specified initial and final heading. The question of reachability naturally arises, since an underwater glider must ascend or descend to locomote. A glider can not progress between two points at the same depth, for example, without concatenating at least one ascending and one descending motion. For the moment, we will restrict our attention to situations in which the final point is strictly below (above) the initial point and can be reached in a single descending (ascending) flight without exceeding the vehicle's physical limitations (such as the minimum glide slope). More precisely, we will project the vehicle path onto the horizontal plane and simply ignore the vertical component of motion. A fortunate consequence of the structure of our approximate solution for turning flight is that, to first order in ϵ, the horizontal and vertical components of velocity remain constant. Thus, the minimum time problem in the horizontal plane corresponds to minimizing the *change in depth* for a given horizontal point-to-point transition. Since an underwater glider propels itself by the force of gravity, minimizing the change in depth is equivalent to minimizing the energy expenditure.

To see that the horizontal component of velocity remains constant, to first order in ϵ, recall that the speed V remains constant to first order in ϵ and note that

$$\begin{aligned}
\dot{z} &= \boldsymbol{e}_3^T \boldsymbol{\mathcal{R}}_{\mathrm{IB}}(\phi,\theta,\psi)\boldsymbol{\mathcal{R}}_{\mathrm{BC}}(\alpha,\beta)\,(V\boldsymbol{e}_1) \\
&= \boldsymbol{e}_3^T \left(e^{\widehat{\boldsymbol{e}}_3\psi} e^{\widehat{\boldsymbol{e}}_2\theta} e^{\widehat{\boldsymbol{e}}_1\phi}\right)\left(e^{-\widehat{\boldsymbol{e}}_2\alpha} e^{\widehat{\boldsymbol{e}}_3\beta}\right)(V\boldsymbol{e}_1) \\
&= \boldsymbol{e}_3^T \left(e^{\widehat{\boldsymbol{e}}_2(\theta_0)} e^{\widehat{\boldsymbol{e}}_1(\epsilon\phi_1+O(\epsilon^2))}\right)\left(e^{-\widehat{\boldsymbol{e}}_2(\alpha_0+O(\epsilon^2))} e^{\widehat{\boldsymbol{e}}_3(\epsilon\beta_1+O(\epsilon^2))}\right)\left((V_0+O(\epsilon^2))\boldsymbol{e}_1\right) \\
&= -V_0 \sin(\theta_0-\alpha_0) + O(\epsilon^2).
\end{aligned}$$

Of course, $-V_0 \sin(\theta_0 - \alpha_0)$ is precisely the vertical component of velocity in unperturbed, wings level flight. An important consequence of this observation is that, since both the magnitude and the vertical component of velocity remain constant, to first order in ϵ, so does the horizontal component of velocity. Projecting the vehicle's motion onto the horizontal plane, glider equilibrium motions correspond to constant-speed straight-line and circular paths. The speed is determined solely by the vehicle net weight and, in practice, may be assumed to take the maximum achievable value. Considering only motion in the horizontal plane, the control problem reduces to the following: *choose the turn rate to minimize the time of transit from a given initial point to a given final point with a specified initial and final heading.*

7.1 Dubins Car

Viewing the glider motion from directly above, the minimum time control problem is reminiscent of Dubins' car [8], a planar vehicle which drives forward at constant speed and which may turn, in either direction, at any rate up to some maximum value. Dubins showed that the minimum time control policy which brings the car from a given point to another, with specified initial and final directions, is a concatenation of three motions: a left or right turn at maximum rate, a straight transit or a second turn at maximum rate, and a final turn at maximum rate. Note that a constant speed turn at maximum turn rate corresponds to a turn of minimum radius. (Actually, Dubins considered the problem in terms of minimizing the length of a continuous curve with limits on the curvature, but the two problems are equivalent.)

Variations of Dubins' problem have enjoyed renewed attention in recent years, in part because of increasing interest in mobile robotics. Reeds and Shepp [24] characterized the family of optimal trajectories for a variation of Dubins' car in which the vehicle could move in reverse, as well as forward. Sussmann and Tang [31] generalized further by "convexifying" the non-convex control set defined in [24], managing to sharpen the results presented by Reeds and Shepp and by Dubins. Parallel studies, as outlined in a series of INRIA technical reports and papers [3, 28, 5, 6], also investigated controllability and optimal path planning for Dubins and Reeds-Shepp mobile robots. Anisi's thesis [1] reviews some of the recent results and provides some historical context.

For the purpose of explaining the Dubins car problem, let $\boldsymbol{x} = [x, y, \psi]^T$ represent the vehicle's state (i.e., its position and heading in the horizontal plane) and let the turn rate $u = r$ be the input, which satisfies the inequality constraint $|r| \leq |r_{\max}|$. The vehicle moves at some constant, nonzero forward speed V. Then the equations of motion are

$$\dot{\boldsymbol{x}} = \boldsymbol{f}(\boldsymbol{x}, u) \qquad \text{where} \qquad \boldsymbol{f}(\boldsymbol{x}, u) = \begin{pmatrix} V\cos\psi \\ V\sin\psi \\ u \end{pmatrix}. \tag{35}$$

Although Dubins problem was originally presented as one of minimizing the arclength of a continuously differentiable curve, it may be re-stated as follows: Find an input history which brings the system from a specified initial state $\boldsymbol{x}(0) = \boldsymbol{x}_0$ to a specified final state $\boldsymbol{x}(t_f) = \boldsymbol{x}_f$ while minimizing $t_f > 0$. Note that, since the speed is constant, this minimum time problem is equivalent to Dubins' minimum arclength problem. Mathematically, the problem may be stated in terms of minimizing the integral

$$\int_0^{t_f} \mathcal{L}(\boldsymbol{x}, u) dt$$

subject to the dynamics (35) where, for this minimum time problem, the "Lagrangian" is

$$\mathcal{L}(\boldsymbol{x}, u) = 1. \tag{36}$$

Using a Lagrange multiplier $\boldsymbol{\lambda}(t)$ in the standard way to augment the cost function with the "dynamic constraint" (35) leads to the following problem: Minimize

$$\int_0^{t_f} \left(\mathcal{H}(\boldsymbol{x}, \boldsymbol{\lambda}, u) + \dot{\boldsymbol{\lambda}}^T \boldsymbol{x} \right) dt - \left[\boldsymbol{\lambda}^T \boldsymbol{x} \right]_{t=0}^{t=t_f}$$

where the "Hamiltonian" is

$$\begin{aligned} \mathcal{H}(\boldsymbol{x}, \boldsymbol{\lambda}, u) &= \mathcal{L}(\boldsymbol{x}, u) + \boldsymbol{\lambda}^T \boldsymbol{f}(\boldsymbol{x}, u) \\ &= 1 + V\lambda_x \cos\psi + V\lambda_y \sin\psi + \lambda_\psi u. \end{aligned} \tag{37}$$

Necessary conditions for optimality of a given control history are that

$$\dot{\boldsymbol{\lambda}} = -\left(\frac{\partial \mathcal{H}}{\partial \boldsymbol{x}} \right)^T \tag{38}$$

and

$$\frac{\partial \mathcal{H}}{\partial u} = 0 \tag{39}$$

along corresponding trajectories. For many optimization problems, equation (39) suggests a candidate optimal control policy u^*. Furthermore, if $\mathcal{H}$ is convex in u with a minimum at u^*, then u^* is indeed the optimal policy. For Dubins' problem, neither is the case; equation (39) fails to provide a candidate optimal control policy and $\mathcal{H}$ is not convex in u. One must therefore appeal to Pontryagin's maximum principle which says that the optimal control u^* is the one which maximizes $\mathcal{H}(\boldsymbol{x}, \boldsymbol{\lambda}, u)$ pointwise in time. Since

$$\mathcal{H}(\boldsymbol{x}, \boldsymbol{\lambda}, u) = 1 + V\lambda_x \cos\psi + V\lambda_y \sin\psi + \lambda_\psi u,$$

the optimal control, in cases where $\lambda_\psi \neq 0$, is

$$u^* = \begin{cases} r_{\max} & \lambda_\psi > 0 \\ -r_{\max} & \lambda_\psi < 0 \end{cases}$$

The former condition corresponds to a turn in the positive direction at maximum rate (minimum turn radius) and the latter corresponds to a turn in the negative direction at maximum rate. These control values are known as "bang-bang" or "maximum effort" values. The case in which $\lambda_\psi \equiv 0$ on some nontrivial interval is singular and Pontryagin's maximum principle fails to provide an optimal control policy. Because $\boldsymbol{\lambda}$ must be a nonzero vector, however, and because (38) indicates that λ_x and λ_y are constant, $\lambda_\psi \equiv 0$ on a time interval if and only if

$$\boldsymbol{\lambda} \parallel \begin{pmatrix} \cos\psi(t) \\ \sin\psi(t) \\ 0 \end{pmatrix}$$

over the interval. This can only be true if $\psi(t)$ remains constant during the interval, in which case the vehicle is travelling a straight path. Thus, for Dubins' car, optimal control histories consist solely of turns at maximum rate and straight paths; that is

$$u^* = \begin{cases} r_{\max} & \lambda_\psi > 0 \\ 0 & \lambda_\psi \equiv 0 \\ -r_{\max} & \lambda_\psi < 0 \end{cases}$$

As shown in [8], the optimal history contains at most three distinct segments (i.e., two switches of the control among its three possible values). These results are sharpened in [31], where the control histories are shown to be of the type "BSB" (for "bang-singular-bang") or "BBB." Representative optimal paths are shown in Figure 8.

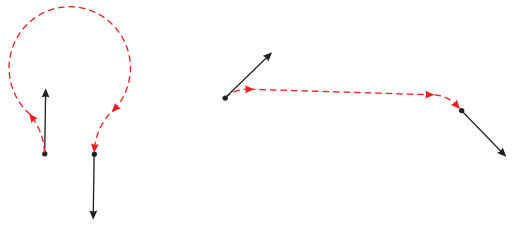

Figure 8: BBB and BSB paths for Dubins' car.

Having characterized the family of candidate optimal input histories, it remains to actually choose the best one for a given initial and final state. Considering, for example, the case where the intermediate transit is a straight path that is much longer than the vehicle turn radius, a simple, geometric algorithm as illustrated in Figure 9 provides the optimal path. One defines two oriented circles of minimum radius that are tangent to the initial velocity vector and two more oriented circles of minimum radius that are tangent to the final velocity vector. Connecting the circles by directed tangents that are consistent with the sense of the circles yields four admissible paths. Because the vehicle moves at constant speed, the path of minimum arclength is the minimum time path.

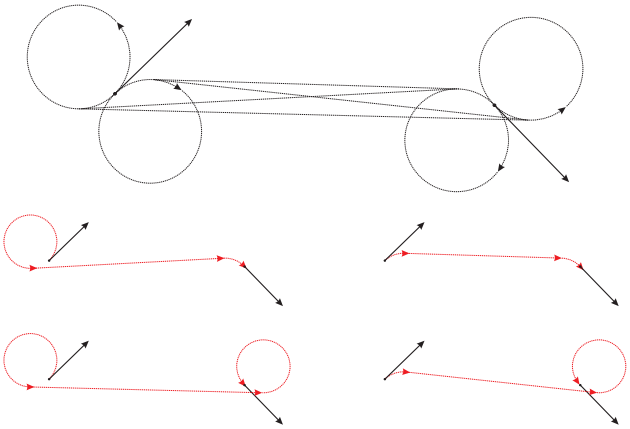

Figure 9: A geometric method for selecting the time-optimal path for Dubins' car when the end-points are more than twice the minimum turn radius apart.

To apply the approach described in Section 7.1 to the underwater glider, assume that the glider is executing some nominal gliding motion at a given glide slope and speed. Given an initial heading, a desired final heading may be attained, at least approximately, by solving the Dubins problem for the horizontal projected motion. Recall that the minimum time problem in the horizontal plane corresponds to minimizing the change in depth, which equates to minimizing the propulsive energy expenditure. This is an appealing feature of Dubins paths, given that underwater gliders are specifically designed for propulsive efficiency.

7.2 Dubins Car with Control Rate Limits

The classical Dubins car problem assumes that turn rate can be treated as an input with magnitude limits but no rate limits. (Equivalently, the arclength minimization problem imposes limits on the curvature but not on its derivative.) The assumption may or may not be appropriate for wheeled robotic vehicles, but it is certainly not appropriate for underwater gliders. For these vehicles, turn rate is controlled indirectly by shifting the center of gravity to effect a banked turn. To explore the effect of control rate limits on the Dubins optimal path result, one may augment the state vector given in Section 7.1 as follows: $\boldsymbol{x} = [x, y, \psi, r]^T$. Let the turn *acceleration* be the input: $u = \dot{r}$ where r satisfies the *state* inequality constraint $|r| \leq |r_{\max}|$ and u satisfies the *input* inequality constraint $|u| \leq |u_{\max}|$. The equations of motion are

$$\dot{\boldsymbol{x}} = \boldsymbol{f}(\boldsymbol{x}, u) \qquad \text{where} \qquad \boldsymbol{f}(\boldsymbol{x}, u) = \begin{pmatrix} V\cos\psi \\ V\sin\psi \\ r \\ u \end{pmatrix}.$$

Although we now consider turn acceleration as an input, we still assume that the underwater glider state varies in a quasi-steady manner. That is, we assume that the vehicle state varies along the continuum of (approximate) equilibrium states, as parameterized by the turn rate. Under this assumption, as shown in Section 5.2, the vehicle's speed V remains constant to first order in turn rate.

In fact, this problem has been treated in some detail by Scheuer [25], as summarized in [26]. Her work extends that of Boissonnat and colleagues [4] and of Kostov and Degtiariova-Kostova [19], who considered the case where the derivative of the turn rate (equivalently, the derivative of curvature) is constrained, but not the magnitude of the turn rate. In [4], it was shown that time-optimal paths exist and that they consist of straight segments and clothoids at maximum turn acceleration. It was also shown that the minimum time curves can be quite complicated, possibly including infinitely many clothoidal segments. Independently, Kostov and Degtiariova-Kostova [19] proposed a method for constructing suboptimal paths from clothoids and straight segments. The term "suboptimal," as used in [19], means that the amount by which the transit time exceeds the minimum time is bounded by a function of the turn acceleration limit.

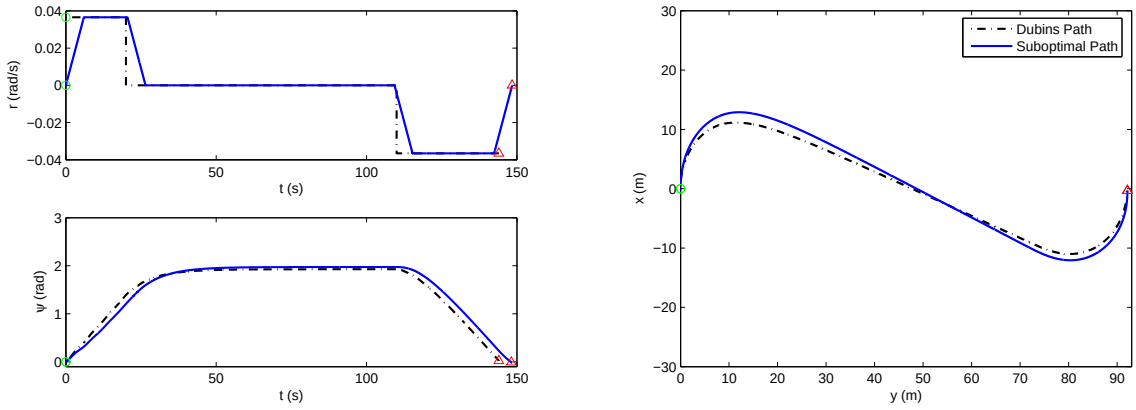

Figure 10: Optimal and suboptimal paths for *Slocum*.

In [26], the authors suggest an intuitive approach for approximating Dubins paths by concatenating

straight, circular, and clothoidal segments. The authors also show that the resulting paths are suboptimal, in the sense described above.

Figure 10 shows the result of a Dubins-type path planning application for the *Slocum* glider considered in Section 6. The objective is to construct an input sequence that brings the glider from a given initial position and heading to a desired final position and heading. The time histories to the left in Figure 10 show the turn rate history and the corresponding heading angle history. Shown at the right is the resulting path, viewed from above. In these simulations, the vehicle travels at a nominal speed of 1.5 knots. The input is the lateral mass location r_{p}. In the first simulation, the input r_{p} is subject to magnitude limits, effectively resulting in turn rate limits; the corresponding path in Figure 10 is labelled as the "Dubins Path." In the second simulation, the input is subject to both magnitude and rate limits, effectively resulting in both turn rate and turn acceleration limits; the corresponding path is labelled as the "Suboptimal Path." Note that the time histories corresponding to the Suboptimal Path are slightly longer than those corresponding to the Dubins Path, as one should expect. It must be emphasized that there is no feedback control in these simulations; here, the dynamics are simply evolving under a sequence of open-loop control commands for r_{p}. A more sophisticated approach, which incorporates actuator dynamics and the feedback control system is discussed in [22].

7.3 Additional Comments on Glider Path Planning

An obvious concern, with regard to the Dubins path planning approach, is that the solution for steady turning motion is only approximate. A motion plan based on this solution will introduce heading error which, integrated over time, may lead to a significant navigation error. One may incorporate feedback to compensate for the error in the approximation, although feedback corrections incur additional energy cost. Another factor which causes disparity between the planned and actual motion is the change in fluid density that occurs when a glider passes between thermal layers. Such changes in density can have a sudden and dramatic effect on a glider's trim speed and attitude. If the thermoclines are known, however, these disturbances can be countered through a combination of feedforward and feedback control.

Ocean currents can also significantly influence a glider's motion, even at depth. Because underwater gliders move quite slowly, relative to conventional AUVs, and operate over much longer time spans, even light currents can have a large, cumulative effect on vehicle motion. The Dubins path planning procedure has recently been extended to the case of a constant ambient current in [23, 32]. In the approach described in these papers, the Dubins path is planned relative to the (moving) ambient fluid with suitably re-defined endpoint conditions. The related question of optimal gliding flight conditions was addressed in [18] for sailplanes in ambient winds. In this study, the authors obtained and experimentally verified conditions for optimal gliding flight (i.e., for the minimum glide path angle). Combining energy-optimal flight conditions with the path planning procedure described in [32], with suitable modifications to allow for turn acceleration limits, could provide a constructive, energy-efficient approach to underwater glider guidance and control.

8 Conclusions

An approximate solution for steady turning motions of underwater gliders has been derived using a sophisticated dynamic model. The problem was formulated as a regular perturbation problem using wings-level, equilibrium flight as the nominal state and turn rate as the small perturbation parameter. As an illustration, the result was applied to an existing model of the *Slocum* underwater glider. The analytical result, though approximate, is quite valuable because it gives better insight into the effect of parameters on vehicle motion and stability. This insight can, in turn, lead to better usage guidelines for current vehicles and design guidelines for future vehicles.

An important observation concerning the structure of the approximate solution is that, to first order in turn rate, the glider's horizontal component of motion matches that of Dubins' car, a classic example in the study of time-optimal paths for mobile robots. Moreover, these minimum time "Dubins paths" yield glider paths which minimize the change in depth, and therefore the change in potential energy. Because gliders use potential energy for propulsion, Dubins paths are essentially energy-optimal paths.

Acknowledgements. The authors gratefully acknowledge P. Bhatta, G. D'Spain, J. Graver, S. Jenkins, N. Leonard, and J. Luby for contributing to our understanding of underwater gliders. The authors are also very grateful to B. Murray, of NSWC-Carderock, for his generous guidance and mentorship in the use of USAERO.

A Added Mass and Added Inertia

This appendix provides a brief description of a computational approach to determining added mass and inertia for autonomous underwater vehicles (AUVs) with complicated geometries. An example application is the *Liberdade/XRay* underwater glider developed jointly by the Scripps Institute of Oceanographys Marine Physical Laboratory and the University of Washingtons Applied Physics Laboratory; see Figure 11. There are many computational, experimental, and semi-empirical techniques for determining forces and moments on a body in a steady viscous flow. Experimental techniques are naturally the most accurate, but are quite costly, particularly during the preliminary design stage when a vehicle's geometry has not yet been fixed. Even after prototype construction, a careful experimental parameter identification program can be prohibitively expensive. Computational techniques are appealing, although the results can be sensitive to uncertainty in critical parameters, such as the point of flow separation. Semi-empirical methods, such as those available in the U.S. Air Force Stability and Control Datcom [33], are commonly used to obtain first-cut estimates of force and moment dependencies

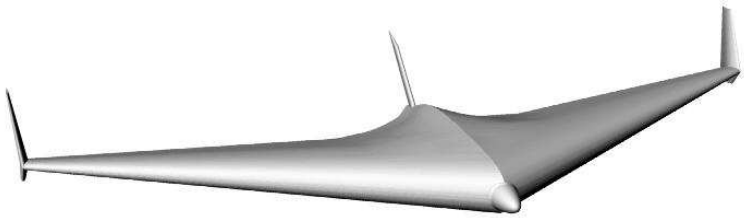

Figure 11: The blended wing-body underwater glider *Liberdade/XRay*. (Solid model in Rhinoceros 3.0)

A more difficult problem, for AUVs, is to determine the generalized added mass (added inertia, added mass, and hydrodynamic inertial coupling). These terms are often called "unsteady" terms, although some effects (such as the "Munk moment") are experienced even in a steady flow. Regardless, to determine all of these parameters requires unsteady experimentation or unsteady computations. The program USAERO, an unsteady flow extension of the popular VSAERO CFD package, allows one to compute these terms. Because added mass is a potential flow effect, the computations essentially involve solving Laplace's equation numerically, although possibly with complicated boundary conditions. The computational results are therefore insensitive to controversial concerns that arise in viscous simulations such as the location of flow separation. (Separation does not occur in a potential flow.)

This Appendix outlines the theory and techniques related to the computation of added mass and inertia, based on the treatment in [20].

Consider a rigid body $\mathcal{B}$ of arbitrary shape immersed in an inviscid, incompressible fluid which is itself contained in some envelope $\mathcal{E}$. Let $\boldsymbol{u}$ denote the velocity of the fluid at a point with respect to some coordinate frame fixed in space. The motion of the fluid bounded between $\mathcal{B}$ and $\mathcal{E}$ is called *irrotational* if the *vorticity* $\nabla \times \boldsymbol{u}$ is zero at every point in the fluid. In this case, the motion of any infinitesimal volume of fluid is described by a combination of pure translation and pure strain; there is no rotational component. Suppose that a closed curve denoted ∂A is drawn within the fluid and that this curve completely bounds a surface A (see Figure 12). The *circulation* of the

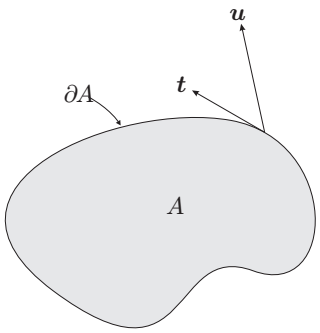

Figure 12: Circulation.

fluid about the circuit ∂A is defined as

$$\Gamma = \int_{\partial A} \boldsymbol{u} \cdot \boldsymbol{t}\, ds$$

where s denotes arclength along the curve and $\boldsymbol{t}$ denotes the unit tangent vector tangent to the curve. By Stokes' theorem,

$$\Gamma = \iint_A (\nabla \times \boldsymbol{u}) \cdot \boldsymbol{n}\, dA$$

where dA represents a differential area element of the surface A and $\boldsymbol{n}$ denotes a unit vector normal to that element. The fluid motion is irrotational if $\Gamma = 0$ about every circuit ∂A that can be drawn in the fluid. Kelvin's circulation theorem states that, in the absence of nonconservative forces, Γ remains constant. Thus if the fluid motion is initially irrotational, it will always be so.

The free, irrotational motion of an ideal fluid in a simply-connected region is described by a single-valued velocity potential ϕ:

$$\boldsymbol{u} = -\nabla\phi. \tag{40}$$

Lamb [20] gives the following physical interpretation for the velocity potential: "Any actual state of motion of a liquid, for which a (single-valued) velocity potential (ϕ) exists, could be produced instantaneously from rest by the application of a properly chosen system of impulsive pressures"

$$\rho\,\phi + C,$$

where ρ is the fluid density and C is an arbitrary constant. (The additive constant has no effect on the fluid motion since it represents a uniformly applied impulsive pressure.) The condition for continuity of an incompressible fluid is that $\nabla \cdot \boldsymbol{u} = 0$ everywhere in the fluid. If the fluid motion derives from a velocity potential, continuity implies that

$$\nabla^2\phi = 0 \tag{41}$$

throughout the fluid. Considering the conditions for solubility of Laplace's equation, the velocity potential is completely determined (up to an additive constant) when ϕ, $\nabla\phi\cdot\boldsymbol{n}$, or some combination is given over the bounding surfaces $\mathcal{E}$ and $\mathcal{B}$. (Following convention, $\boldsymbol{n}$ denotes the unit normal vector to the surface directed *into* the fluid.) If the envelope $\mathcal{E}$ extends to infinity, it is sufficient to require that the velocity be zero there. In this case, too, the fluid motion is completely determined.

Let $\mathcal{E}/\mathcal{B}$ denote the fluid volume. Recalling equation (40) for the fluid velocity, assuming that ϕ satisfies (41), and applying the divergence theorem to the quantity $\boldsymbol{u}\phi$ gives

$$\iiint_{\mathcal{E}/\mathcal{B}} \|\nabla\phi\|^2\, dV = -\iint_{\mathcal{E}} \phi\nabla\phi \cdot \boldsymbol{n}\, dA - \iint_{\mathcal{B}} \phi\nabla\phi \cdot \boldsymbol{n}\, dA. \tag{42}$$

The kinetic energy of the fluid is

$$\mathrm{KE_f} = \frac{1}{2}\iiint_{\mathcal{E}/\mathcal{B}} \rho \| \boldsymbol{u} \|^2 \, dV, \tag{43}$$

so premultiplying both sides of equation (42) by $\frac{1}{2}\rho$ reveals an energy balance,

$$\mathrm{KE_f} = -\frac{1}{2}\rho \left(\iint_{\mathcal{E}} \phi \nabla\phi \cdot \boldsymbol{n} dA + \iint_{\mathcal{B}} \phi \nabla\phi \cdot \boldsymbol{n} dA \right). \tag{44}$$

According to Lamb's interpretation of the velocity potential, the right-hand side of (44) represents the work done by the system of impulsive pressures which, applied at the bounding surfaces, would effect the actual fluid motion from a state of rest.

Of particular interest is the case in which the rigid body $\mathcal{B}$ moves through the fluid under no influence other than that of the fluid. In this case, the "work" done by the rigid body on the fluid, i.e., the right-hand side of (44), takes a simple form. By treating the body and the fluid as one combined dynamical system, the partial differential equations which describe the more general problem of rigid body motion in a fluid reduce to a finite set of ordinary differential equations and, as Lamb remarks, "the troublesome calculation of the effect of the fluid pressures on the surfaces of the solids is avoided."

Suppose that the surface of the envelope $\mathcal{E}$ is infinitely far from the rigid body $\mathcal{B}$ in all directions. Fix a coordinate frame to $\mathcal{B}$ and suppose that the body moves with translational velocity $\boldsymbol{v} = [u, v, w]^T$ and angular velocity $\boldsymbol{\omega} = [p, q, r]^T$, both written with respect to the moving coordinate frame. (See Figure 13.) Consider the problem of finding a velocity potential ϕ which satisfies Laplace's equation

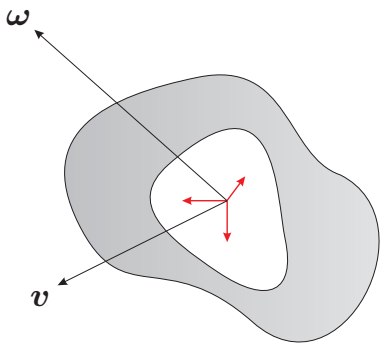

Figure 13: Rigid body in a fluid.

(41) subject to the conditions that

1. the fluid velocity normal to the surface of $\mathcal{B}$ at a point is equal to the normal velocity of the surface at that point.
2. the fluid is at rest infinitely far from $\mathcal{B}$.

Tangential motion of the fluid at the body's surface is allowed but is not prescribed. Kirchhoff found that the solution takes the form

$$\phi = \boldsymbol{v} \cdot \boldsymbol{\phi} + \boldsymbol{\omega} \cdot \boldsymbol{\chi} \tag{45}$$

where the components of $\boldsymbol{\phi} = [\phi_1, \phi_2, \phi_3]^T$ and $\boldsymbol{\chi} = [\chi_1, \chi_2, \chi_3]^T$ depend only on the shape of $\mathcal{B}$. Let $\boldsymbol{x}$ denote the position of a point on the surface of the rigid body relative to the body-fixed coordinate frame. The boundary condition at the surface of $\mathcal{B}$ becomes

$$-\nabla\phi \cdot \boldsymbol{n} = (\boldsymbol{v} + \boldsymbol{\omega} \times \boldsymbol{x}) \cdot \boldsymbol{n}. \tag{46}$$

Each component of $\boldsymbol{\phi}$ and $\boldsymbol{\chi}$ must satisfy equation (41) independently, subject to the relevant boundary condition on $\mathcal{B}$ implied by equation (46) with ϕ given by (45):

$$-\nabla\boldsymbol{\phi} \cdot \boldsymbol{n} = -\begin{pmatrix} \nabla\phi_1 \cdot \boldsymbol{n} \\ \nabla\phi_2 \cdot \boldsymbol{n} \\ \nabla\phi_3 \cdot \boldsymbol{n} \end{pmatrix} = \boldsymbol{n} \qquad \text{and} \qquad -\nabla\boldsymbol{\chi} \cdot \boldsymbol{n} = -\begin{pmatrix} \nabla\chi_1 \cdot \boldsymbol{n} \\ \nabla\chi_2 \cdot \boldsymbol{n} \\ \nabla\chi_3 \cdot \boldsymbol{n} \end{pmatrix} = \boldsymbol{\chi} \times \boldsymbol{n}.$$

According to Lamb, Lord Kelvin defines the 'impulse' of the body-fluid system at an instant to be the impulsive force and couple required to instantaneously generate the body and fluid's motion from rest. Lamb shows that the component of impulse due to the pressure at the infinite boundary $\mathcal{E}$ vanishes and that the variation in system impulse is therefore given entirely by the time integral of the external forces acting on the rigid body. The system impulse thus behaves "in exactly the same way as the momentum of a finite dynamical system."

Let $\boldsymbol{p} = [p_1, p_2, p_3]^T$ and $\boldsymbol{h} = [h_1, h_2, h_3]^T$ represent the impulsive force and couple, respectively, written with respect to the body-fixed coordinate frame. Also, let $\boldsymbol{f}_{\text{other}}$ and $\boldsymbol{m}_{\text{other}}$ represent an external force and torque acting on the rigid body. As Lamb shows by considering infinitesimal motions of the body-fluid system, the impulse varies according to the equations

$$\begin{aligned} \dot{\boldsymbol{h}} &= \boldsymbol{h} \times \boldsymbol{\omega} + \boldsymbol{p} \times \boldsymbol{v} + \boldsymbol{m}_{\text{other}} \\ \dot{\boldsymbol{p}} &= \boldsymbol{p} \times \boldsymbol{\omega} + \boldsymbol{f}_{\text{other}}. \end{aligned}$$

Since the integral over $\mathcal{E}$ vanishes, the kinetic energy of the fluid (44) becomes

$$\text{KE}_{\text{f}} = -\frac{1}{2}\rho \left(\iint_{\mathcal{B}} \phi \nabla\phi \cdot \boldsymbol{n} \, dA \right). \tag{47}$$

Substituting the expression (45) for the velocity potential ϕ into (47) gives

$$\text{KE}_{\text{f}} = \frac{1}{2} \begin{pmatrix} \boldsymbol{v} \\ \boldsymbol{\omega} \end{pmatrix}^T \begin{pmatrix} \boldsymbol{M}_{\text{f}} & \boldsymbol{C}_{\text{f}}^T \\ \boldsymbol{C}_{\text{f}} & \boldsymbol{I}_{\text{f}} \end{pmatrix} \begin{pmatrix} \boldsymbol{v} \\ \boldsymbol{\omega} \end{pmatrix} \tag{48}$$

where the square matrix is a constant, symmetric, positive definite matrix whose entries depend only upon the density of the fluid and the shape of the body $\mathcal{B}$. For example,

$$\begin{aligned} \boldsymbol{M}_{\text{f}_{xx}} &= -\rho \iint_{\mathcal{B}} \phi_1 \nabla\phi_1 \cdot \boldsymbol{n} \, dS \\ &= \rho \iint_{\mathcal{B}} \phi_1 (\boldsymbol{n} \cdot \boldsymbol{e_1}) \, dS, \end{aligned}$$

where the latter equality arises from the boundary condition (46). The expression (48) for the fluid kinetic energy holds formally for bodies $\mathcal{B}$ of arbitrary shape. Naturally, the complexity of the integrals defining the components of $\boldsymbol{M}_{\text{f}}, \boldsymbol{C}_{\text{f}}$, and $\boldsymbol{I}_{\text{f}}$ depends on the complexity of the shape of the body and on the choice of body-fixed coordinate frame.

Let $\mathrm{KE}_{\mathrm{rb}}$ denote the kinetic energy of the rigid body. It is assumed that the mass of the body, say m, is equal to the mass of the displaced fluid so that the body is neutrally buoyant. The location of the mass center of $\mathcal{B}$ with respect to the body-fixed coordinate frame is given by $\boldsymbol{r}$. Let $\boldsymbol{I}_{\mathrm{rb}}$ denote the rigid body inertia tensor computed with respect to the body-fixed frame. Then the kinetic energy of the rigid body alone is

$$\mathrm{KE}_{\mathrm{rb}} = \frac{1}{2}\begin{pmatrix} \boldsymbol{v} \\ \boldsymbol{\omega} \end{pmatrix}^T \begin{pmatrix} m\mathbb{1} & -m\hat{\boldsymbol{r}} \\ m\hat{\boldsymbol{r}} & \boldsymbol{I}_{\mathrm{rb}} \end{pmatrix} \begin{pmatrix} \boldsymbol{v} \\ \boldsymbol{\omega} \end{pmatrix}, \tag{49}$$

where $\hat{\boldsymbol{a}}\boldsymbol{b} = \boldsymbol{a} \times \boldsymbol{b}$ for vectors $\boldsymbol{a}$ and $\boldsymbol{b}$. The total system energy is

$$\mathrm{KE} = \mathrm{KE}_{\mathrm{rb}} + \mathrm{KE}_{\mathrm{f}} = \frac{1}{2}\begin{pmatrix} \boldsymbol{v} \\ \boldsymbol{\omega} \end{pmatrix}^T \begin{pmatrix} \boldsymbol{M} & \boldsymbol{C}^T \\ \boldsymbol{C} & \boldsymbol{I} \end{pmatrix} \begin{pmatrix} \boldsymbol{v} \\ \boldsymbol{\omega} \end{pmatrix} \tag{50}$$

where

$$\begin{aligned} \boldsymbol{M} &= \boldsymbol{M}_{\mathrm{f}} + m\mathbb{1} \\ \boldsymbol{C} &= \boldsymbol{C}_{\mathrm{f}} + m\hat{\boldsymbol{r}} \\ \boldsymbol{I} &= \boldsymbol{I}_{\mathrm{f}} + \boldsymbol{I}_{\mathrm{rb}}. \end{aligned} \tag{51}$$

Lamb shows that the system impulse is related to the rigid body velocity according to

$$p_i = \frac{\partial T}{\partial v_i} \qquad \text{and} \qquad h_i = \frac{\partial T}{\partial \omega_i} \tag{52}$$

for $i = 1, 2$, and 3. In terms of the system impulse, the total kinetic energy is

$$\mathrm{KE} = \frac{1}{2}\begin{pmatrix} \boldsymbol{p} \\ \boldsymbol{h} \end{pmatrix}^T \begin{pmatrix} \boldsymbol{M} & \boldsymbol{C}^T \\ \boldsymbol{C} & \boldsymbol{I} \end{pmatrix}^{-1} \begin{pmatrix} \boldsymbol{p} \\ \boldsymbol{h} \end{pmatrix}. \tag{53}$$

Lamb points out several simplifications of the generalized inertia tensor. For example, one may always rotate the body coordinate axes such that $\boldsymbol{M}$ becomes diagonal. Furthermore, writing $\boldsymbol{C}$ as the sum of a symmetric and a skew-symmetric matrix, one may eliminate the skew-symmetric contribution by shifting the coordinate origin. Thus the number of coefficients required to define the generalized inertia reduces from twenty-one to fifteen. Further simplifications follow for particular body shapes. In particular, Lamb discusses bodies having one or more planes of symmetry, one or more axes of symmetry, and a special type of "helicoidal" symmetry illustrated by a ship's propeller. An ellipsoid with uniformly distributed mass is an example of a body with three planes of symmetry. Choosing coordinate axes fixed to the ellipsoid principal axes, one finds that $\boldsymbol{M} = \mathrm{diag}(m_1, m_2, m_3)$, $\boldsymbol{C} = \boldsymbol{0}$, and $\boldsymbol{I} = \mathrm{diag}(I_1, I_2, I_3)$. Even if the ellipsoid mass is not uniformly distributed, one obtains such simplifications for the added mass and inertia matrices $\boldsymbol{M}_{\mathrm{f}}$, $\boldsymbol{C}_{\mathrm{f}}$, and $\boldsymbol{I}_{\mathrm{f}}$.

With these definitions, the momenta $\boldsymbol{h}$ and $\boldsymbol{p}$ are related to the velocities $\boldsymbol{\omega}$ and $\boldsymbol{v}$ through the *generalized inertia matrix* as follows:

$$\begin{pmatrix} \boldsymbol{p} \\ \boldsymbol{h} \end{pmatrix} = \begin{pmatrix} \boldsymbol{M} & \boldsymbol{C}^T \\ \boldsymbol{C} & \boldsymbol{I} \end{pmatrix} \begin{pmatrix} \boldsymbol{v} \\ \boldsymbol{\omega} \end{pmatrix}. \tag{54}$$

The dynamic equations, attributed to Kirchhoff, which relate external forces and moments to the rate of change of linear and angular momentum are

$$\dot{\boldsymbol{p}} = \boldsymbol{p} \times \boldsymbol{\omega} \tag{55}$$

$$\dot{\boldsymbol{h}} = \boldsymbol{h} \times \boldsymbol{\omega} + \boldsymbol{p} \times \boldsymbol{v}. \tag{56}$$

Numerical computations of added mass and inertia terms for underwater gliders, using unsteady, invsicid flow code, are described in [12].

References

[1] D. A. Anisi. Optimal motion control of a ground vehicle. Technical Report FOI-R–0961–SE, Swedish Defence Research Agency, Stockholm, Sweden, July 2003.

[2] P. Bhatta. *Nonlinear Stability and Control of Gliding Vehicles*. PhD thesis, Princeton University, 2006.

[3] J.-D. Boissonnat, A. Cérézo, and J. Leblond. Shortest paths of bounded curvature in the plane. In *IEEE International Conference on Robotics and Automation*, pages 2315–2320, Nice, France, May 1992.

[4] J.-D. Boissonnat, A. Cérézo, and J. Leblond. A note on shortest paths in the plane subject to a constraint on the derivative of the curvature. Technical Report 2160, Institut National de Recherche en Informatique et en Automatique (INRIA), January 1994.

[5] J.-D. Boissonnat X.-N. Bui. Accessibility region for a car that only moves forwards along optimal paths. Technical Report 2181, Institut National de Recherche en Informatique et en Automatique (INRIA), January 1994.

[6] X.-N. Bui, J.-D. Boissonnat, P. Souéres, and J.-P. Laumond. Shortest path synthesis for dubins non-holomic robot. In *IEEE International Conference on Robotics and Automation*, San Diego, CA, May 1994.

[7] R. E. Davis, C. C. Eriksen, and C. P. Jones. Autonomous buoyancy-driven underwater gliders. In G. Griffiths, editor, *Technology and Applications of Autonomous Underwater Vehicles*, volume 2, chapter 3. Taylor and Francis, 2002.

[8] L. E. Dubins. On curves of minimal length with a constraint on average curvature and with prescribed initial and terminal positions and tangents. *American Journal of Mathematics*, 79, 1957.

[9] C. C. Eriksen, T. J. Osse, R. D. Light, T. Wen, T. W. Lehman, P. L. Sabin, J. W. Ballard, and A. M. Chiodi. Seaglider: A long-range autonomous underwater vehicle for oceanographic research. *Journal of Oceanic Engineering*, 26(4):424–436, 2001. Special Issue on Autonomous Ocean-Sampling Networks.

[10] B. Etkin and L.D. Reid. *Dynamics of Flight Stability and Control*. John Wiley and Sons,Inc., New York, 1996.

[11] T. I. Fossen. *Guidance and Control of Ocean Vehicles*. John Wiley and Sons, 1995.

[12] J. S. Geisbert. Hydrodynamic modeling for autonomous underwater vehicles using computational and semi-empirical methods. Master's thesis, Virginia Polytechnic Institute & State University, Blacksburg, VA, June 2007.

[13] J. G. Graver. *Underwater Gliders: Dynamics, Control, and Design*. PhD thesis, Princeton University, 2005.

[14] J. G. Graver, J. Liu, C. A. Woolsey, and N. E. Leonard. Design and analysis of an underwater glider for controlled gliding. In *Conference on Information Sciences and Systems*, pages 801–806, 1998.

[15] J. Guckenheimer and P. Holmes. *Nonlinear Oscillations, Dynamical Systems, and Bifurcations of Vector Fields*. Springer-Verlag, New York, NY, 1983.

[16] P. Hartman. *Ordinary Differential Equations*. John Wiley and Sons, Inc., New York, NY, 1964.

[17] S. A. Jenkins, D. E. Humphreys, J. Sherman, J. Osse, C. Jones, N. Leonard, J. Graver, R. Bachmayer, T. Clem, P. Carroll, P. Davis, J. Berry, P. Worley, and J. Wasyl. Underwater glider system study. Technical Report 53, Scripps Institution of Oceanography, May 2003.

[18] S. A. Jenkins and J. Wasyl. Optimization of glides for constant wind fields and course headings. *Journal of Aircraft*, 27(7):632–638, 1990.

[19] V. Kostov and E. Degtiariova-Kostova. The planar motion with bounded derivative of the curvature and its suboptimal paths. Technical Report 2189, Institut National de Recherche en Informatique et en Automatique (INRIA), January 1994.

[20] H. Lamb. *Hydrodynamics*. Dover, New York, NY, sixth edition, 1932.

[21] N. E. Leonard and J. G. Graver. Model-based feedback control of autonomous underwater gliders. *Journal of Oceanic Engineering*, 26(4):633–645, 2001. Special Issue on Autonomous Ocean-Sampling Networks.

[22] N. Mahmoudian and C. A. Woolsey. Underwater glider motion control. In *IEEE Conference on Decision and Control*, pages 552 – 557, Cancun, Mexico, December 2008.

[23] T. G. McGee and J. K. Hedrick. Optimal path planning with a kinematic airplane model. *Journal of Guidance, Control, and Dynamics*, 30(2):629–633, 2007.

[24] J. A. Reeds and L. A. Shepp. Optimal paths for a car that goes both forwards and backwards. *Pacific Journal of Mathematics*, 145(2):367–393, 1990.

[25] A. Scheuer. *Planification de chemin à courbure continue pour robot mobile non-holonome*. PhD thesis, Institut National Polytechnique de Grenoble, 1998.

[26] A. Scheuer and Ch. Laugier. Planning sub-optimal and continuous-curvature paths for car-like robots. In *IEEE/RSJ International Conference on Intelligent Robots and Systems*, pages 25–31, Victoria, B.C., Canada, October 1998.

[27] J. Sherman, R. E. Davis, W. B. Owens, and J. Valdes. The autonomous underwater glider "Spray". *Journal of Oceanic Engineering*, 26(4):437–446, 2001. Special Issue on Autonomous Ocean-Sampling Networks.

[28] P. Souéres, J.-Y. Fourquet, and J.-P. Laumond. Set of reachable positions for a car. *IEEE Transactions on Automatic Control*, 39(8):1626–1630, August 1994.

[29] R. F. Stengel. *Flight Dynamics*. Princeton University Press, Princeton, NJ, 2004.

[30] Brian L. Stevens and Frank L. Lewis. *Aircraft control and simulation, Second Ed.* John Wiley and Sons, INC., Hoboken, N.J., 2003.

[31] H. J. Sussmann and G. Tang. Shortest paths for the Reeds-Shepp car: A worked out example of the use of geometric techniques in nonlinear optimal control. Technical Report 91-10, Rutgers University Center for Systems and Control, New Brunswick, NJ, 1991.

[32] L. Techy, C. A. Woolsey, and III D. G. Schmale. Path planning for efficient UAV coordination in aerobiological sampling missions. In *IEEE Conference on Decision and Control*, pages 2814–2819, Cancun, Mexico, December 2008.

[33] USAF. *Stability and Control Datcom*. Air Force Flight Dynamics Lab, 1978.

[34] D. C. Webb, P. J. Simonetti, and C. P. Jones. SLOCUM: An underwater glider propelled by environmental energy. *Journal of Oceanic Engineering*, 26(4):447–452, 2001. Special Issue on Autonomous Ocean-Sampling Networks.